MODELING OF DEFORMATIONS OF SINGLE-WALLED CARBON NANOTUBES

A Dissertation

Presented to the Faculty of the Graduate School

of Cornell University

in Partial Fulfillment of the Requirements for the Degree of

Doctor of Philosophy

by

Chao Fang

August 2012

MODELING OF DEFORMATIONS OF SINGLE-WALLED CARBON NANOTUBES

Chao Fang, Ph.D.

Cornell University 2012

This thesis presents a study of single-walled carbon nanotubes (SWNTs) using revised Cosserat rod models. A SWNT is a thin hollow cylinder, with diameter of the order of 1 *nm* and length possibly as large as 1μm. Its wall is composed of a single layer of carbon atoms with an estimated thickness around 0.335 *nm*. A single walled CNT (SWNT) is classified as armchair, zig-zag or chiral, depending on the (regular) arrangement of atoms on its surface.

In general, CNT models based on traditional continuum mechanics can be inconsistent or inaccurate [57, 44, 16], while atomistic simulations can be prohibitively expensive. Atomistic-continuum models e.g. the quasi-continuum approach, originally proposed for bulk crystals [47, 51], attempt to combine the accuracy of atomistic simulations with the efficency of continuum models. This approach has been applied to CNTs [61, 26, 8, 9, 7, 10, 2, 55, 11].

At relatively long length scales, it makes sense to propose a one-dimensional model for a SWNT. For such long nanotubes, one-dimensional models are attractive for both theoretical modeling as well as numerical simulation. Chandraseker et al. [10] proposed a Cosserat rod model [1] for a SWNT that can capture large deformations of SWNTs. This model includes deformation modes such as bending, twisting, extension and shear, as well as coupling between ex-

tension and twist and between shear and bending. Kumar and Mukherjee [31] futher developed the Cosserat rod model to incorporate cross-sectional deformation and allow coupling between cross-sectional deformation with twist and extension.

In this work, finite element simulations of both standard and revised Cosserat rod models are carried out. Using a standard Cosserat rod model combined with atomistic simulation, the governing equations of a rod model are tranformed into weak form and discritized. The weak form of the govening equations contain both geometric and material nonlinearity. A implicite iterative method, based on the Newtown-Raphson method is performed to find the converged solution. Several numerical verification cases are performed to validate the method and demostrate the capability of this numerical implementation. Finally, in the case of the revised Cosserat rod model, a similar process is carried out to find the finite element solution. In this case, material property is assumed to be linear and only geometric nonlinearity is incoporated.

Finally, a mathematically consistent extension to the revised rod theory is developed that connects an isotropic and hemitropic rod by exploring material symmetry. This proposed approach is applied to model SWNTs with different chiralities. It effectively connects the modeling of different types of SWNTs using five material parameters. The connection between different types of SWNTs is controlled by the chirality angle in the this derivation. Future effort could involve solving the inverse problem to find these material parameters.

BIOGRAPHICAL SKETCH

Chao Fang was born on Jan 23, 1985 in Jiaozuo, Henan Province, China. His father was a retired Chinese army officer and his mother was a administration staff in Jiaozuo Teacher's College. He lived in Jiaozuo for eighteen years before moving to Beijing for college. After finishing his high school in Jiaozuo No.1 Middle School, he joined Beijing University of Aeronautics and Astronautics in 2003 for his undergraduate in Aeronautical Science and Engineering. In BUAA, he learned about aircraft as well as foundamental mechanics and numerical simulation methods. Following his graduation from BUAA in 2007, he came to the USA to pursue his PhD in the Field of Theoretical and Applied Mechanics which now is housed in the School of Mechanical and Aerospace Engineering at Cornell University. He started his research on modeling of single walled carbon nanotubes with Professor Subrata Mukherjee, the following year. Upon his graduation from Cornell University, Chao will pursue his career as a research engineer in the software industry.

To my parents

ACKNOWLEDGEMENTS

My five years as a Ph.D. student at Cornell is the most exciting yet challenging phase of my career so far. During this time, I acquired a significant amount of knowlege from many brilliant scholars. I learned to be independent both in life and career. I feel priviledged to dedicate this part of my thesis as special thanks to all who have supported me.

I thank my advisor, Prof. Subrata Mukherjee for his constant effort in teaching me and leading me into exciting research projects. He is so kind and helpful as my mentor and friend. I couldn't have completed this work without his help. It was under his mentorship that I formed the interest and skills in research. I am also very thankful to him for his tireless work on many of my writings. He is like a parent of mine giving me directions not only in academic work but also in life and career.

I would like to thank Dr. Ajeet Kumar who taught me rod theory and constantly helped with my research. He is a good friend. His great insight into rod theory and dedication to research set a good example for me. I enjoy discussing research problems with him and always get inspired. I am also thankful to Dr. Kathick Chandraseker who pioneered my research project and also gave a lot of advice for my research.

I would also like to thank Professor Alan Zehnder for teaching me continuum mechanics and giving me valuable advice for my research. Thanks are also due to Professor Charles Van Loan who taught me to organize computation in matrix way.

I would also like to thank Professor Wolfgang Sachse, Professor Andy Ruina, Professor Herbert Hui and Dr. Petru Patrina for the help with my teaching. Teaching was a great experience during my time at Cornell. I would also like to express my appreication to Dr. Jingzhou Liu, Dr. Haolin Zhu and Dr. Rong Long for discussing research problems and life in Ithaca.

Thanks to Dan Mittler, Cindy Twardokus, Polly Marion and Corie Scott for their help with administrative and techniqual support and making all the things in a smooth way.

I cannot thank enough all the people who made my Ph.D studies a great experience in my life. Many thanks to my friends Chao Ding, Ying Cao who shared the same flight and then the five years journey at Cornell. I am also thankful to Xinwei Wu, Songming Peng, Yuerui Lu, Han Wang, Yu Zhao and Xi Yan for woking with me in Cornell CSSA 2009. Together, we are proud of being the most successful leadership team in Cornell CSSA history.

TABLE OF CONTENTS

LIST OF TABLES

LIST OF FIGURES

CHAPTER 1

INTRODUCTION

Modeling of deformation of a carbon nanotube (CNT) has been a popular topic of research in recent years (see, e.g., [10], [2]-[56]). A CNT is a thin hollow cylinder, with diameter of the order of 1 *nm* and length possibly as large as $1\mu m$. Its wall is composed of a single layer of carbon atoms with an estimated thickness around 0.335 *nm*. A single walled CNT (SWNT) is classified as armchair, zig-zag or chiral, depending on the (regular) arrangement of atoms on its surface.

Chandraseker et al., in a recent paper [10], have proposed an atomistic-continuum model based on Coserat rod theory, for deformation (extension, twist, shear and bending) of a chiral SWNT. A quadratic representation of strain energy density for a chiral SWNT was used here. This representation was proposed earlier for a chiral rod in [22].

The second Chapter of this thesis addresses FEM analysis of SWNT rods subjected, in general, to axial and transverse loads, as well as bending moments and torques. The FEM model uses the aforementioned quadratic strain energy density representation from Ref.[22]. Derivation of the weak form is analogous to Refs.[48] and [31]. As a result, geometrical nonlinearities are included in the FEM model, while material nonlinearities are included by virtue of the fact that the parameters in the strain energy expression are strain dependent. Also, as a consequence of the adopted strain energy density expression, the SWNT is anisotropic.

An interesting conclusion of [10] was that the SWNT with bending modulus

B_R, was much more flexible in bending compared to a 'simple' beam with otherwise identical geometrical and material properties, but with a bending modulus YI (Young's modulus× Section area moment of inertia) based on standard continuum mechanics (according to [10], $B_R = .0168YI$, see also, [44]). However, in a recent paper [41], the authors conclude from experimental observation and post-processing of their experimental data, that $B_r \approx EI$ (within experimental scatter). Section 6 of the second Chapter revisits [41] and argues that this conclusion in [41] may be wrong!

The second chapter is organized as follows: In Section 2, we discusses the kinematics of the Cosserat rod model and the hyperelastic constitutive model. In Section 3, the weak form of the governing equation is derived. Section 3 is followed by a detailed discussion of the treatment of material nonlinearity of a carbon nanotube. Section 5 presents several numerical examples. Section 6 revisits a recent paper [41]. A concluding remarks section completes the Chapter.

Gould and Burton [20] proposed a modified Cosserat rod model with deformable cross-sections. In addition to failing to capture the Poisson coupling between axial stretch and cross-sectional shrinkage, their model was also limited to isotropic and linear material behavior. Their model also assumes that the deformation of a cross-section is decoupled from other deformation modes such as bending, twisting or axial stretching of the tube. To address these limitations, Kumar and Mukherjee [31] proposed a new rod model that allows deformation of cross-sections. Using symmetry arguments, they also derived its quadratic strain energy density form which accounts for all the relevant coupling modes reported in Chandraseker et al. [10]. In addition, it also accounts for the pres-

ence of coupling between cross-sectional and other deformation modes such as the Poisson coupling between axial stretch and cross-sectional shrinkage and coupling between twist and cross-sectional shrinkage. The quadratic strain energy density in this model has 12 parameters. These parameters are obtained in Kumar et al. [32]. It is important to mention here that the results reported in Kumar et al. [32] has an important limitation, i.e., periodic boundary conditions imposed in the Tight Binding Density Function (DFTB) simulations suppress any induced twist that is typically generated when a chiral nanotube is axially stretched. As a result, the extension-twist coupling parameter turns out to be nearly zero. The value of this parameter is recalculated in the present work.

The third Chapter presents a FEM implementation of (9,6) chiral and (10,10) armchiar SWNTs using a modified Cosserat rod model that also allows its cross-sections to deform [31, 32]. Kinematics of the model is presented first. This is followed by a discussion of the weak form of the governing equations. Numerical results for several examples follow next where the emphasis is placed on (1) coupling between extension, twist and cross-sectional deformation and (2) global buckling of a (10,10) Chiral SWNT. A concluding remarks section completes this Chapter.

The last Chapter presents an analytical study of reduced moduli for a revised Cosserat rod model. By exploring material symmetry of SWNTs, the twelve rod parameters can be reduced to five material parameters and chirality angle together with cross-section integrals. This approach not only reduces the number of parameters but also provide an explicit relationship between different types of rod chiralities. Using this result, we can use one set of parameters to model

all types of SWNTs.

CHAPTER 2

FINITE ELEMENT ANALYSIS OF SINGLE-WALLED CARBON NANOTUBES BESED ON AN ATOMISTIC-CONTINUUM COSSERAT ROD MODEL

2.1 Kinematics and Strain Measures of a Cosserat Rod Model

This section presents the kinematics of static deformation of Cosserat rods. The definition of strain measures and the associated physical explanations are discussed.

In a rod model [20, 1], an undeformed configuration of the rod is definded in a global fixed coordinate with the orthonormal basis$\{\mathbf{e_1}, \mathbf{e_2}, \mathbf{e_3}\}$. The undeformed rod is straight and parallel to $\mathbf{e_3}$ with plane cross sections. Let s denote the arc-length coordinate for the undeformed rod. Then, $\mathbf{r}(s)$ and $\mathbf{R}(s)$ are defined as the configuration variables with $\mathbf{r}(s)$ the position vector of the centerline and $\mathbf{R}(s)$ is the rotation matrix of the cross section.

When the rod has not deformed:

$$\mathbf{r(s)} = \mathbf{se_3}, \qquad \mathbf{R(s)} = \begin{bmatrix} 1 & 0 & 0 \\ 0 & 1 & 0 \\ 0 & 0 & 1 \end{bmatrix} \tag{2.1}$$

A moving frame with orthonormal basis $\{\mathbf{d_1}, \mathbf{d_2}, \mathbf{d_3}\}$ called directors are defined with $\{\mathbf{d_1}, \mathbf{d_2}\}$ span the cross section:

$$\mathbf{d}_i(s) = \mathbf{R}(s)\mathbf{e}_i; \qquad i = 1, 2, 3 \tag{2.2}$$

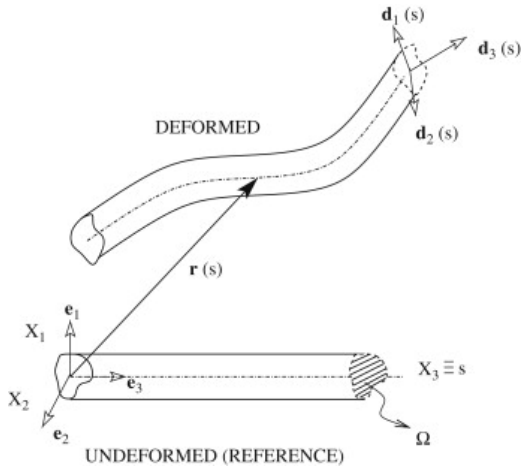

Figure 2.1: The kinematic description of a Cosserat rod [10]

Then the deformed configuration is uniquely expressed by $\mathbf{r}(s)$ and $\mathbf{R}(s)$ (see Fig.2.1). By differentiation of (2.2) with respect to s, we have

$$\mathbf{d}_i^{'} = \mathbf{R}^{'}\mathbf{R}^T\mathbf{d}_i; \qquad i = 1, 2, 3 \tag{2.3}$$

Since $\mathbf{R}^{'}\mathbf{R}^T$ is a skew-symmetric tensor, there exists a unique vector

$$\boldsymbol{\kappa} = \kappa_i\mathbf{d}_i; \qquad i = 1, 2, 3 \tag{2.4}$$

such that:

$$\mathbf{d}_i^{'} = \boldsymbol{\kappa} \times \mathbf{d}_i; \qquad i = 1, 2, 3 \tag{2.5}$$

Similarly, differentiating $\mathbf{r}(\mathbf{s})$ with respect to s yields

$$\mathbf{r}_i^{'} = \nu_i\mathbf{d}_i; \qquad i = 1, 2, 3 \tag{2.6}$$

Here, κ_i and ν_i are 'strains'[1]. Specificly, κ_1 and κ_2 represent 'bending' and κ_3 is 'twist', ν_1 and ν_2 are 'shear' and ν_3 is 'stretch'. For a hyperelastic rod, a strain energy function can be defined as[22]

$$\Phi = \int_0^L W(\nu_1, \nu_2, \nu_3, \kappa_1, \kappa_2, \kappa_3)ds \tag{2.7}$$

We define triples $\underline{\nu} = \nu_1, \nu_2, \nu_3$ and $\underline{\kappa} = \kappa_1, \kappa_2, \kappa_3$. Now, we can obtain the internal contact force $\mathbf{n} = n_i \mathbf{d}_i$ and internal moment $\mathbf{m} = m_i \mathbf{d}_i$

$$n_i = \frac{\partial W(\underline{\nu}, \underline{\kappa})}{\partial \nu_i}, \qquad m_i = \frac{\partial W(\underline{\nu}, \underline{\kappa})}{\partial \kappa_i} \qquad i = 1, 2, 3 \tag{2.8}$$

Equation (2.8) is the constitutive equation of the rod model.

2.2 Weak Form of Governing Equations and Linearization

To implement the finite element method, we need to find the weak form of the balance equations. Generally, two approaches can be used. One is multiplying the balance equation with an arbitrary admissible variation of displacement and then integrating by parts to get the weak form. The other method is by variation of the stationary potential energy. Here, we use the second approach to obtain the weak form. First we perturb the configuration of a rod about an arbitrary equilibrium configuration ($\mathbf{r}(s)$ and $\mathbf{R}(s)$)

$$\mathbf{r}_\epsilon = \mathbf{r} + \epsilon \Delta \mathbf{r}, \qquad \mathbf{R}_\epsilon = exp(\epsilon \Delta \mathbf{\Theta}) \mathbf{R} \tag{2.9}$$

Here, $\Delta \mathbf{\Theta}$ denotes an admissible, skew-symetric matrix and we can find the axial vector $\Delta \boldsymbol{\theta}$ of it. As in Simo and Quoc[48], $\mathbf{R}_\epsilon$ denotes a SO(3) proper rotation. Then neglecting higher order terms, the strain measures are expressed as:

$$\begin{aligned}
\boldsymbol{\nu}_\epsilon &= \mathbf{R}_\epsilon^T \mathbf{r}_\epsilon^{'} \\
&= (exp(\epsilon \Delta \mathbf{\Theta}) \mathbf{R})^T (\mathbf{r} + \epsilon \Delta \mathbf{r})^{'} \\
&= \mathbf{R}^T (\mathbf{I} - \epsilon \Delta \mathbf{\Theta} + \frac{\epsilon^2}{2} \Delta \mathbf{\Theta}^2 + \cdots)(\mathbf{r}^{'} + \epsilon \Delta \mathbf{r}^{'}) \\
&\approx \boldsymbol{\nu} + \epsilon \mathbf{R}^T (\Delta \mathbf{r}^{'} - \Delta \boldsymbol{\theta} \times \mathbf{r}^{'}) + \frac{\epsilon^2}{2} \mathbf{R}^T (\Delta \boldsymbol{\theta} \times (\Delta \boldsymbol{\theta} \times \mathbf{r}^{'}) - 2 \Delta \boldsymbol{\theta} \times \Delta \mathbf{r}^{'})
\end{aligned} \tag{2.10}$$

$$
\begin{aligned}
\boldsymbol{\kappa}_\epsilon &= axial(\mathbf{R}_\epsilon^T \mathbf{R}_\epsilon^{'}) \\
&= axial(\mathbf{R}^T exp(-\epsilon\Delta\boldsymbol{\Theta})((\epsilon\Delta\boldsymbol{\Theta}^{'} + \epsilon^2\Delta\boldsymbol{\Theta}^{'}\Delta\boldsymbol{\Theta})\mathbf{R} + exp(\epsilon\Delta\boldsymbol{\Theta})\mathbf{R}^{'})) \\
&\approx \boldsymbol{\kappa} + \epsilon\mathbf{R}^T\Delta\boldsymbol{\theta}^{'} + \frac{\epsilon^2}{2}\mathbf{R}^T(\Delta\boldsymbol{\theta}^{'} \times \Delta\boldsymbol{\theta})
\end{aligned} \tag{2.11}
$$

Taking the variation of the strain energy expression (2.7) with respect to ϵ, one gets the weak form:

$$
\begin{aligned}
G &\equiv \frac{d\Phi}{d\epsilon}|_{\epsilon=0} \\
&= \int_0^L (\frac{\partial W}{\partial \boldsymbol{\nu}} \cdot \frac{d\boldsymbol{\nu}_\epsilon}{d\epsilon} + \frac{\partial W}{\partial \boldsymbol{\kappa}} \cdot \frac{d\boldsymbol{\kappa}_\epsilon}{d\epsilon})ds \\
&= \int_0^L (\frac{\partial W}{\partial \boldsymbol{\nu}} \cdot (\mathbf{R}^T(\Delta\mathbf{r}^{'} - \Delta\boldsymbol{\theta} \times \mathbf{r}^{'})) + \frac{\partial W}{\partial \boldsymbol{\kappa}} \cdot \mathbf{R}^T\Delta\boldsymbol{\theta}^{'})ds \\
&= \int_0^L (\mathbf{n} \cdot \Delta\mathbf{r}^{'} + \mathbf{m} \cdot \Delta\boldsymbol{\theta}^{'} + (\mathbf{r}^{'} \times \mathbf{n}) \cdot \Delta\boldsymbol{\theta})ds
\end{aligned} \tag{2.12}
$$

Now, following Simo's notation, we use the variables $\boldsymbol{\eta}_0$ and $\boldsymbol{\psi}$ instead of $\Delta\mathbf{r}$ and $\Delta\boldsymbol{\theta}$. Here $\boldsymbol{\eta}_0$ and $\boldsymbol{\psi}$ correspond to smooth variations of $\mathbf{r}$ and $\mathbf{R}$, respectively. Then the weak form becomes:

$$
G \equiv \int_0^L (\mathbf{n} \cdot \boldsymbol{\eta}_0^{'} + \mathbf{m} \cdot \boldsymbol{\psi}^{'} + (\mathbf{r}^{'} \times \mathbf{n}) \cdot \boldsymbol{\psi})ds \tag{2.13}
$$

It should be noted that this weak form is only valid for Dirichlet boundary conditions (or free boundary conditions). There will be additional boundary terms in the linearlized part of G for non-conservative problems[48].

The next step is to linearlize the weak form. In order to do this, we perform similar perturbations of the configuration $\mathbf{r}$ and $\mathbf{R}$ to get $\mathbf{r}_\epsilon = \mathbf{r} + \epsilon\Delta\mathbf{r}$ and $\mathbf{R}_\epsilon = exp(\epsilon\Delta\boldsymbol{\Theta})\mathbf{R}$. Then, using Taylor expansion, we get:

$$
G(\mathbf{r}_\epsilon, \mathbf{R}_\epsilon) = G(\mathbf{r}, \mathbf{R}) + \epsilon DG(\mathbf{r}, \mathbf{R}) \begin{bmatrix} \Delta\mathbf{r} \\ \Delta\boldsymbol{\theta} \end{bmatrix} + o|\epsilon \begin{bmatrix} \Delta\mathbf{r} \\ \Delta\boldsymbol{\theta} \end{bmatrix}|. \tag{2.14}
$$

For numerical convenience, we rewrite (3.15) in discrete form. Following Simo[48], $DG(\mathbf{r}, \mathbf{R}) \begin{bmatrix} \Delta\mathbf{r} \\ \Delta\boldsymbol{\theta} \end{bmatrix}$ is called the tangent stiffness. First the following quan-

tities are defined:

$$\mathbf{C}_{(6\times6)} = \begin{bmatrix} \frac{\partial^2 W}{\partial \underline{\mathbf{v}}^2} & \frac{\partial^2 W}{\partial \underline{\mathbf{v}} \partial \underline{\mathbf{k}}} \\ \frac{\partial^2 W}{\partial \underline{\mathbf{k}} \partial \underline{\mathbf{v}}} & \frac{\partial^2 W}{\partial \underline{\mathbf{k}}^2} \end{bmatrix}, \quad \Pi_{(6\times6)} = \begin{bmatrix} \mathbf{R} & \mathbf{0} \\ \mathbf{0} & \mathbf{R} \end{bmatrix}, \quad \mathbf{E}^T_{(6\times6)} = \begin{bmatrix} \mathbf{1}\frac{d}{ds} & \mathbf{r}'\times \\ \mathbf{0} & \mathbf{1}\frac{d}{ds} \end{bmatrix}$$

Thus, the discretized tangent stiffness is presented in matrix form[31]:

$$DG(\mathbf{r},\mathbf{R}) \begin{bmatrix} \Delta\mathbf{r} \\ \Delta\boldsymbol{\theta} \end{bmatrix} \equiv \int_0^L [\mathbf{\Pi C \Pi}^T \mathbf{E}^T \begin{bmatrix} \Delta\mathbf{r} \\ \Delta\boldsymbol{\theta} \end{bmatrix} \cdot \mathbf{E}^T \begin{bmatrix} \boldsymbol{\eta_0} \\ \boldsymbol{\psi} \end{bmatrix} + \begin{bmatrix} \mathbf{0} & -\mathbf{n}\times \\ \mathbf{0} & -\mathbf{m}\times \end{bmatrix} \begin{bmatrix} \Delta\mathbf{r}_0 \\ \Delta\boldsymbol{\theta_0} \end{bmatrix} \cdot \mathbf{E}^T \begin{bmatrix} \boldsymbol{\eta_0} \\ \boldsymbol{\psi} \end{bmatrix} + (\mathbf{n} \times \Delta\mathbf{r}') \cdot \boldsymbol{\psi}] ds \tag{2.15}$$

The first term in (3.16) is due to linearization of the internal force. We write it below as the material part of the tangent stiffness matrix:

$$\int_0^L \left[\mathbf{\Pi C \Pi}^T \mathbf{E}^T \begin{bmatrix} \Delta\mathbf{r} \\ \Delta\boldsymbol{\theta} \end{bmatrix} \cdot \mathbf{E}^T \begin{bmatrix} \boldsymbol{\eta_0} \\ \boldsymbol{\psi} \end{bmatrix} \right] ds \tag{2.16}$$

where $\mathbf{C}$ is the elasticity tensor.

The second term is the geometric part of the tangent stiffness matrix:

$$\int_0^L \left[\begin{bmatrix} \mathbf{0} & -\mathbf{n}\times \\ \mathbf{0} & -\mathbf{m}\times \end{bmatrix} \begin{bmatrix} \Delta\mathbf{r}_0 \\ \Delta\boldsymbol{\theta}_0 \end{bmatrix} \cdot \mathbf{E}^T \begin{bmatrix} \boldsymbol{\eta_0} \\ \boldsymbol{\psi} \end{bmatrix} + (\mathbf{n} \times \Delta\mathbf{r}') \cdot \boldsymbol{\psi} \right] ds \tag{2.17}$$

Now that we have the tangent stiffness matrix, Newton's method, together with the finite element method (FEM) is used to solve this nonlinear problem. We use linear shape functions for the finite element formulation which will ensure C_1 continuity. We will discuss the treatment of material nonlinearity in the following section.

2.3 Material Nonlinearity of a Carbon Nanotube

A carbon nanotube is considered to be a transversely hemitropic rod with flip symmetry about the axis within the cross-section. Then the strain energy density function up to quadratic terms, can be written as [22]:

$$W = \frac{1}{2}[A\kappa_\alpha\kappa_\alpha + B\kappa_3^2 + C\nu_\alpha\nu_\alpha + D\varepsilon^2 + 2E\varepsilon\kappa_3 + 2F\nu_\alpha\kappa_\alpha] \tag{2.18}$$

Here, the coefficients A,B,C and D are bending, twisting, shearing and extensional 'moduli', E is the extension-twist coupling coefficient, and F is the bending-shear coupling coefficient. Also, $\epsilon = \nu_3 - 1$ (the extensional strain). The following conditions are required for positive-definiteness

$$A, B, C, D > 0, \qquad BD - E^2 > 0, \qquad AC - F^2 > 0 \tag{2.19}$$

This quadratic form of the strain energy density yields the following form of the elasticity tensor $\mathbf{C}$.

From (2.18), the matrix form of the elasticity tensor is:

$$\mathbf{C}_{(6\times6)} = \begin{bmatrix} C & 0 & 0 & F & 0 & 0 \\ 0 & C & 0 & 0 & F & 0 \\ 0 & 0 & D & 0 & 0 & E \\ F & 0 & 0 & A & 0 & 0 \\ 0 & F & 0 & 0 & A & 0 \\ 0 & 0 & E & 0 & 0 & B \end{bmatrix} \tag{2.20}$$

In (2.20), the diagonal terms A,B,C and D are the primary moduli. We can convert them into usual moduli as in Table.2.1.

Table 2.1: A, B, C, D in terms of the usual moduli

A	B	C	D
B_R	GJ	SA_c	YA_c

In Table.2.1, Y is the Young's modulus, G is the twist modulus and S is the shear modulus. Also, J is polar moment of inertia and A_C is the area of cross-section. In [10], the bending stiffness B_R was found to be only 1.68% of the bending stiffness obtained from using the Bernoulli-Euler beam theory (Young's modulus (Y)× bending moment of inertia(I)). Chandrasekar et al. also show that the coupling moduli are small compared to the direct ones and the induced coupling is fairly small compared to the global deformation. In this paper, we will assume there is no coupling effect. Then the coupling constants vanish, i.e. $E = F = 0$. Using modulii, the elasticity tensor finally becomes diagonal with:

$$\mathbf{C}_{(6\times6)} = diag[SA_c, SA_c, YA_c, B_R, B_R, GJ] \tag{2.21}$$

As a consequence of the assumption of quadratic strain energy, which is a simplified model, all of the modulii above become functions of elastic strain generated during the deformation. This material nonlinearity is carefully investigated for a chiral (9×6) single-walled carbon nanotube (SWNT) in [10]. Here we show the nonlinear behavior of the Young's modulus(Y), shear modulus(S), twist modulus(G) and bending modulus(Br) in Fig.2.2 which contains data from [10]. The Young's modulus Y of a cabon nanotube decreases from 1100GPa to 750GPa for a large extension of 25%. The twist modulus stays around 418GPa until κ_3 reaches 0.2 and then decreases almost linearly. The bending stiffness increases moderately as the bending curvature goes up. The shear modulus also

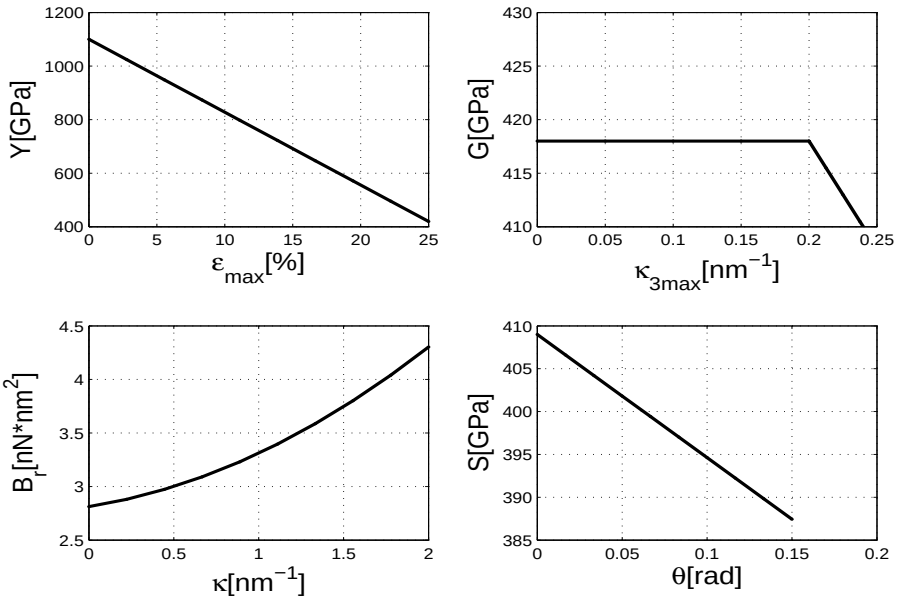

Figure 2.2: Variation of various moduli with generalized strain

drops from 408GPa to 398GPa as a nanotube is being twisted. It should be noted that here we replot the bending stiffness with respect to bending curvature for numerical convenience (The x axis is the mid-point deflection of a nanotube in Fig.11 of [10]). This plot in Fig.2.2 is only valid for diameter .1*nm* but can be recalculated for other diameters.

2.4 Examples

In this section, several examples are presented using our nonlinear finite element solver. In the first example, we validate our code by calculating a well known deformed configuration. The second example is a carbon nanotube cantilever beam subjected to a constant transverse force at its free end. The result is compared with a simple continuum rod model with the same geometry. The third example is the deflection of a carbon nanotube with material nonlinearity.

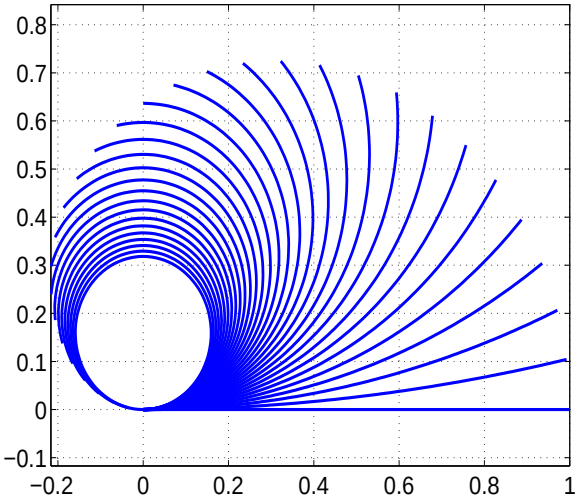

Figure 2.3: Deforming trajectories of a cantilever beam subjected to an increasing end moment

In the last example, we calculate a three-dimensional deformation of a carbon nanotube under complicated loading.

2.4.1 In plane Pure Bending of Simple Cantilever Beam

Simo and Vu-Quoc[48] have used this example to compare their numerical results with the exact solution. Here, we repeat the test to validate our solver. A cantilever beam with unit length is subjected to a uniform bending moment M. The bending stiffness of this beam is 1. When $M = 4\pi$, the beam should deform into a a full closed circle. The bending trajectory is shown in Fig.2.3. In this trajectory, each deformed configuration corresponds to an incremental bending moment of $M/30$.

2.4.2 Carbon Nanotube Cantilever Beam

This example is devised to emphasize the significant low bending stiffness of a carbon nanotube (only 1.68% of YI).Assume that we have a carbon nanotube with one end clamped and the other end free. The carbon nanotube has a length of 100nm, the mean diameter of the cross section is 1nm and its wall thickness is 0.335nm. To observe the low bending stiffness of the carbon nanotube, we compare it with bending of a 'simple beam' the bending stiffness of which is YI. We load the beam with 1pN transverse force. Since the bending stiffness of the carbon nanotube is about 1.68% of YI, if there is a point force of 1pN on the free end of the beam, then the deflection of simple beam should be around 1.68%[10] of the deflection of the carbon nanotube under this relatively small load (assuming most of the beam deflection is due to bending).

The numerical result in Fig.2.4 shows that under the 1pN load, the end deflection of a simple beam is 0.0289nm and the end deflection of the cabon nanotube is 1.7184nm; the ratio is 0.01679. This is in good agreement with the predicted value 1.68%

2.4.3 Static Deflection of Carbon Nanotube

In this example, we investigate the material nonlinearity of a carbon nanotube. The carbon nanotube is modeled as a doubly clamped beam. The beam is 100nm long, with a mean diameter of 1nm for the cross-section and 0.335nm for the wall thickness. In this model, the Young's modulus, bending stiffness, shearing stiff-

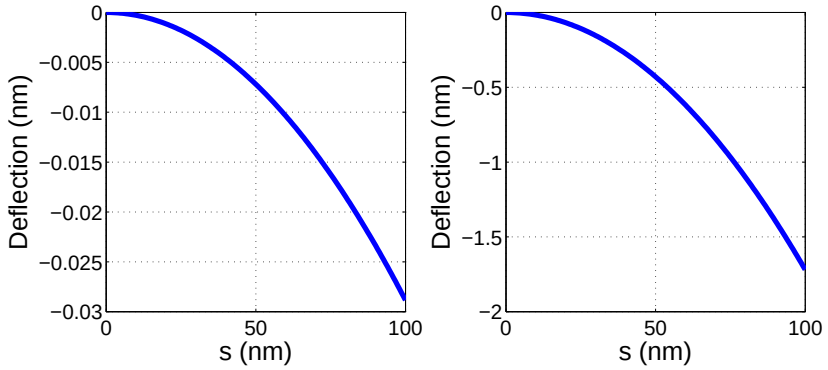

Figure 2.4: The comparison of simple beam deflection (left) with carbon nanotube deflection (right)

ness and torsional stiffness are considered to be nonlinear as shown in Fig.2.2. The nanotube is subjected to a single point load of $0.1pN$ at its mid-point. We compare the deflections of (1) a materially nonlinear CNT, (2) a CNT model without material nonlinearity and (3) a 'simple' beam model.

As shown in Fig.2.5, under the same load $0.1pN$, the simple beam deflects much less compared to the other two models. It can be explained by the fact tha the 'simple' beam has much higher bending stiffness than the other two. On the other hand, the nonlinear behavior of the material properties accounts for the difference between the materially linear CNT and the materially nonlinear CNT. It should be noted that the central deflection $\delta_{simple} \neq 1.68\%\delta_{CNT}$ because this is not pure bending.

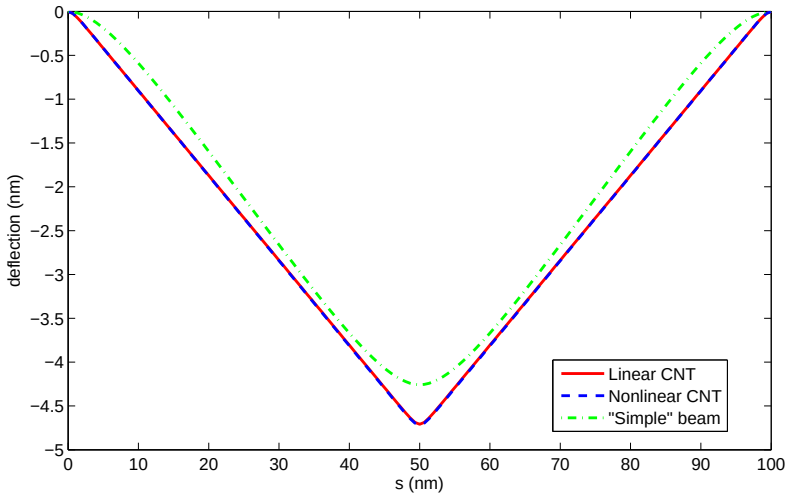

Figure 2.5: Comparison of materially nonlinear CNT deflection (lowest) with materially linear CNT deflection (middle) and simple beam deflection (top)

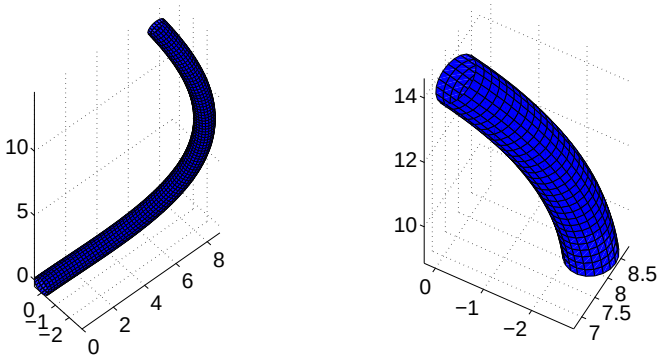

Figure 2.6: Three dimensional deflection of a materially nonlinear CNT. The left figure is the whole deformed configuration and the right figure is a snap shot of the right end of the CNT

2.4.4 Three Dimensional Deflection of Nonlinear CNT

This example demonstrates three dimensional deflection of a materially nonlinear CNT. The left end of a carbon nanotube is considered as a fixed end for all

six degrees of freedoms. The right end is free. The length of the nanotube is $10nm$ and the cross-section parameters are the same as in the last example. On the free end of this CNT, we apply the following loads:

$$\mathbf{F}_1 = 1[pN]\mathbf{e}_1, \qquad \mathbf{F}_2 = 2[pN]\mathbf{e}_2, \qquad \mathbf{F}_3 = -1[pN]\mathbf{e}_3,$$

$$\mathbf{M}_1 = -200[pN \cdot nm]\mathbf{e}_1, \quad \mathbf{M}_2 = -200[pN \cdot nm]\mathbf{e}_2, \quad \mathbf{M}_3 = -200[pN \cdot nm]\mathbf{e}_3$$

Fig.2.6 shows the deformed configuration under the above loads. The deformation consists of bending, shear, stretch(compression) and twist. The material nonlinearity is also included in this example. Here, $\mathbf{F}_k$, $\mathbf{M}_k$ are external forces and moments in the appropriate directions.

2.5 Revisit Ref.[41]

The FEM model developed above is used to revisit the conclusions regarding the bending stiffness B_R of a SWNT in[41]. In [41], the authors conclude that Br is of the order YI(from continuum theory for beam bending). It is felt by the authors of the present paper that this conclusion in [41] is wrong. The reasons for this observation are given below.

Table.2.2 and Table.2.3 summarize the results for a beam (of hollows cylindrical cross section) of length 3000 nm, mean diameter 3 nm and wall thickness 0.337 nm, clamped at both ends and subjected to a central transverse load P. The central deflection δ of the beam, from a linear strength of materials, bending solution ($\delta = \frac{Pl^3}{192YI}$), and from the FEM solutions for a simple beam and a CNT, are

given in this table for various values of the load P. Also given are the partitions of energy, for the simple beam and the CNT, from the FEM solutions, for these cases. The FEM solutions include geometric nonlinearities but are materially linear. The following observations are made:

- Very small load (P = .00001 and .0001pN): Most of the energy, for both the simple beam and CNT, is in bending. The deflections from the analytical solution and the simple beam FEM solution are nearly equal, but the CNT has much higher deflection since it has a much smaller bending stiffness.
- Small loads (P = .001 and .01pN): Most of the energy for the simple beam is still in the bending mode, while the CNT has much of the energy in the stretching mode. The deflections from the analytical and the simple beam solutions, as expected, remain essentially the same. The ratio of $\delta_{cnt}/\delta_{simple}$ decreases as more and more of the CNT deflection becomes stretching dominated.
- load=1pN (approximately the same as in the experiment): Around 60% of the energy for the simple beam is now in the stretching mode, while for the CNT, almost all of the energy is in the stretching mode. Consequently, $\delta_{cnt}/\delta_{simple}$ = 1.17. while, due to memberane stiffening, the central deflection of the simple beam is only about 23% of that from the analytical (bending) solution. The CNT deformation is dominated by stretching. It is practically insensitive to the bending stiffness and it is not a good idea to try to determine the bending stiffness of the CNT from the experiment using the measured central deflection in this case.
- Large loads (P=10 and 100pN): Most of the energy, for both the simple beam and the CNT, is now in the stretching mode. $\delta_{cnt}/\delta_{simple} \rightarrow 1$ while

Table 2.2: Midpoint deflection carbon nanotube under central transverse loads

central force[pN]	Analytical[nm]	Simple beam(FEM)[nm]	CNT(FEM)[nm]	$\delta_{CNT}/\delta_{simple}$
.00001	.00035	.00036	.021	61.76
.0001	.0035	.0036	.193	54.75
.001	.036	.036	.774	21.41
.01	.362	.360	1.941	5.40
.1	3.617	2.648	4.421	1.67
1	36.173	8.319.	9.759	1.17
10	361.732	19.901	21.265	1.06
100	3617.316	44.72	46.056	1.03

Table 2.3: Energy partition of simple beam(columns 2, 3, 4) and CNT(columns 5, 6, 7)(%)(From FEM solution)

central force[pN]	Bending	Extension	Shear	Bending	Extension	Shear
.00001	99.84	0.00	0.16	99.93	0.07	0.00
.0001	99.84	0.00	0.16	94.54	5.46	0.00
.001	99.84	0.00	0.16	53.92	46.08	0.00
.01	99.50	0.34	0.16	21.31	78.69	0.00
.1	84.67	15.33	0.00	9.00	90.98	0.01
1	39.78	60.21	0.02	3.97	95.98	0.05
10	15.82	84.18	0.00	1.80	98.20	0.00
100	6.85	93.14	0.01	0.84	99.16	0.00

the linear analytical bending solution grossly over predicts the central deflection. This phenomenon is called membrane stiffening.

2.6 Concluding Remarks

A FEM model for deformation of SWNTs, subjected to axial and transverse forces, bending moments and torques, is presented in this paper. This analysis is based on a quadratic expression (2.18) for strain energy per unit undeformed length. The resulting constitutive model for the SWNT is anisotropic. Geometric and material nonlinearities are included in this model. Finally, a recent experimental paper is revisted using the solver developed in this paper.

One assumption made in this work, following standard Cosserat rod theory, is that the cross-section of a SWNT remains rigid during deformation. This assumption is not accurate since cross-section deformation of CNTs has been observed [39]. Also, Simo and Vu-Quoc[49] and Gold and Burton[20] have considered cross-sectional deformation of rods. The next Chapter will discuss a revised Cosserat rod model with cross-sectional deformation.

CHAPTER 3

FINITE ELEMENT ANALYSIS OF SINGLE-WALLED CARBON NANOTUBES BASED ON A ROD MODEL INCLUDING IN-PLANE CROSS-SECTIONAL DEFORMATION

3.1 Kinematics and Strain Measures for a Rod Model Including Deformation of Its Cross-sections

This section presents the knematics of static deformation of a rod model including deformation of its cross-sections [31, 32]. The definition of strain measures and the associated physical explanations are discussed below.

The rod model proposed by Kumar et al. [32] can be described as an extension to the special Cosserat theory of rods [1]. The model in Kumar and Mukherjee [31] allows the cross-section to deform anisotropically and also undergo in-plane cross-sectional shearing. Let $\{\mathbf{e}_1, \mathbf{e}_2, \mathbf{e}_3\}$ denote a fixed, right-handed, orthonormal basis for $\mathbf{R}^3$. The coordinates of a material point on the rod in its straight state reference configuration are denoted with $\mathbf{X} = (X_1, X_2, s)$. Here, X_1, X_2 describe the cross-sectional coordinates and s is the arc-length coordinate of the centerline of the rod in its reference configuration.

Here, the deformation map for this rod model can be written as:

$$\mathbf{x}(\mathbf{X}) = \mathbf{r}(s) + X_\alpha \mathbf{d}_\alpha(s) \tag{3.1}$$

In this expresssion, $\mathbf{r}$ represents the position of the centerline of a rod while $\mathbf{d}_\alpha$, in which α sums from 1 to 2, represent two directors on a cross-section in the de-

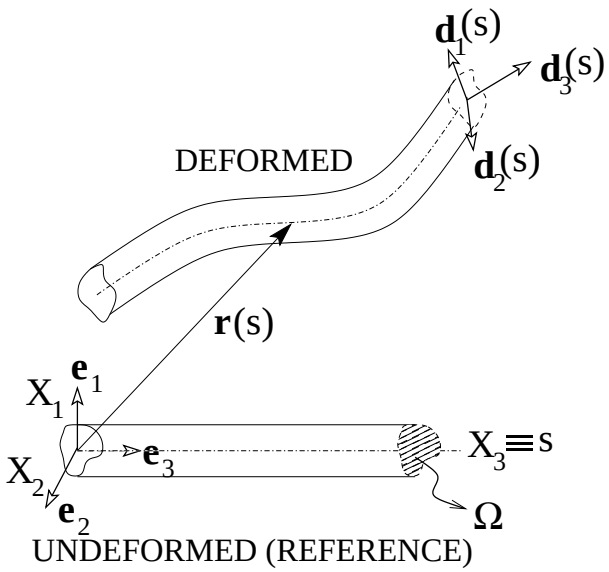

Figure 3.1: A typical rod undergoing deformation from its straight state reference configuration

formed configuration. Fig.3.1 shows both the undeformed and deformed shape of a rod. The two directors $\mathbf{d}_\alpha$ that span a cross-section are allowed to become non-orthogonal after deformation. The deformation map for the directors can be written as:

$$\mathbf{d}_i(s) = \mathbf{R}(s)\mathbf{U}(s)\mathbf{e}_i, \quad \text{for } i = 1, 2, 3 \tag{3.2}$$

This transformation could be decomposed into a product of the three dimensional rigid rotation of a cross-section (**R**) and its in-plane cross-sectional deformation (**U**). The matrix **U** is symmetric and positive definite. The matrix form is shown in the expression (3.3) below. This is an improvement from standard Cosserat rod theory in which **U** is taken to be the identity. This transformation (3.3) keeps the third director unit-normed and perpendicular to the cross-section.

$$\mathbf{U}(s) = \begin{bmatrix} a(s) & c(s) & 0 \\ c(s) & b(s) & 0 \\ 0 & 0 & 1 \end{bmatrix} \tag{3.3}$$

Here, the eigenvectors of the matrix **U** define the two directions in which the cross-section is stretched. The magnitude of this stretch is defined by the respective eigenvalue of the matrix **U**. By introducing the **U** matrix, the cross-section is allowed to become an ellipse with its axes aligned along the eigenvectors of **U**. Here, c is a scalar representing in-plane cross-sectional shearing or "degree of non-orthogonality" of the cross-sectional directors. Orientation of the axes of ellipses is also governed by c. In cases when c is zero, a and b are the positive scalars that represent stretching of the two cross-sectional directors. These three new field variables are responsible for lateral surface deformations of a rod.

The strain measures in this rod model are obtained from the deformation gradient. Here, $\underline{\mathrm{v}} = \mathbf{R}^T\mathbf{r}'$ is a 3-vector ($\underline{\mathrm{v}} = [\nu_1, \nu_2, \nu_3]^T$), the first two components of which represent shear while the third component represents axial stretch. Similarly, $\mathbf{K} = \mathbf{R}^T\mathbf{R}'$ is a skew symmetric matrix whose axial vector $\underline{\mathrm{k}}$ ($\underline{\mathrm{k}} = [\kappa_1, \kappa_2, \kappa_3]^T$) is also a 3-vector, the first two components of which represent components of the local bending curvature while the third component represents twist. There are additional strain measures due to deformation of a cross-section:

$$\underline{\mathrm{z}} = \begin{bmatrix} a \\ b \\ c \end{bmatrix} \quad \text{and} \quad \underline{\mathrm{z}}' = \begin{bmatrix} a' \\ b' \\ c' \end{bmatrix}. \tag{3.4}$$

The strains $\underline{\mathrm{z}}'$ only appear for the case that the cross-section is non-uniformly deformed. The strain energy density per unit of undeformed length can now be

written as a function of these strain measures as:

$$\Phi(\underline{v}, \underline{k}, \underline{z}, \underline{z}', s) = \int_{\Omega} W(\mathbf{F}, s) d\Omega \tag{3.5}$$

Here, W denotes the strain energy per unit of undeformed volume, $\mathbf{F}$ denotes deformation gradient, and Ω denotes the undeformed cross-section of a rod. Healey [22] proposed that the strain energy density be assumed to be quadratic. Kumar and Mukherjee [31], using symmetry arguments, derived the mathematical form of the strain energy density per unit undeformed length for a chiral rod; the same is shown below for the sake of completeness.

$$\begin{aligned}\Phi_{chiral}(.) = \frac{1}{2}\Big[& A\kappa_\alpha\kappa_\alpha + B\kappa_3^2 + C\nu_\alpha\nu_\alpha + D(\nu_3 - 1)^2 + 2E(\nu_3 - 1)\kappa_3 + 2F\nu_\alpha\kappa_\alpha + \\ & 2G(\nu_3 - 1)\left(\frac{a+b}{2} - 1\right) + 2H\kappa_3\left(\frac{a+b}{2} - 1\right) + I\left(\frac{a+b}{2} - 1\right)^2 + \\ & J\left\{(a-1)(b-1) - c^2\right\} + K\left(\frac{a'+b'}{2}\right)^2 + L\left(a'b' - c'^2\right)\Big]\end{aligned} \tag{3.6}$$

The physical meanings of the twelve parameters in (3.6) are as follows:

- A: bending modulus
- B: twist modulus
- C: shear modulus
- D: axial stretch modulus
- E: coupling coefficient between extension and twist
- F: coupling coefficient between shear and bending
- G: Poisson coupling between axial stretch and average cross-sectional stretch
- H: Poisson type coupling between twist and average cross-sectional stretch

- I: average cross-sectional stretch/ cross-sectional size modulus
- J: cross-sectional area change (of 2^{nd} order) modulus
- K, L: penalty for variation in the cross-sectional strains a, b and c along the length of a rod

In case of achiral or isotropic rods, the coupling terms (E, F, H) in (3.6) would vanish. The coupling between twist and average cross-sectional stretch (corresponding to the parameter H) is a new type of coupling for chiral rods. Often, rods are assumed to be unshearable [30] and, in this case, the terms corresponding to C and F in (3.6) can be neglected. Invoking strong ellipticity from nonlinear elasticity, the parameters in the energy expression (3.6) can be shown to satisfy the following inequality constraints in order for a rod to be materially stable [30, 31]. These inequality constraints were derived in Kumar and Mukherjee [31] and are also shown below:

- A>0, B>0, C>0, D>0, I>0, J<0, K> 0, L<0
- AC-F^2 >0, BD-E^2 >0, K> |L|

The quadratic strain energy density from (3.6) contains twelve parameters. The six parameters (A-F) were estimated for a $(9, 6)$ carbon nanotube by Chandraseker et al. [10]. The remaining six parameters (G-L) were estimated by Kumar et al. [32]. The values of the material parameters for a (9,6) and a (10,10) SWNT, used in the present paper, are given in Table 3.1. It is noted that the values of the (9,6) parameters in Table 3.1 have been obtained from two different sources - DFTB and Tersoff-Brenner potential. For example, the value of the extension-twist coupling parameter E for a (9,6) SWNT, which was nearly zero from DFTB, has been revised using the Tersoff-Brenner potential [33]. The

Parameter	Physical meaning	Value (9,6)	Value (10,10)	Units
A	Bending modulus	7.405	829.9	$Ha \times$ Å
B	Twist modulus	480.946	391.9	$Ha \times$ Å
C	Shear modulus	10.195	7.3	Ha/Å
D	Axial stretch modulus	31.02	28.19	Ha/Å
E	Coupling coefficient : extension and twist	0.8257	0.0	Ha
F	Coupling coefficient : shear and bending	0	0.0	Ha
G	Poisson coupling : axial and x secn. stretch	9.91	11.7	Ha/Å
H	Coupling : twist and x secn. stretch	-0.6124	0.0	Ha
I	Average cross-sectional stretch modulus	52.5	45.5	Ha/Å
J	Change of cross-sectional area modulus	-17.9	-17.3	Ha/Å
K	Penalty for variation in x secn. strains	163.4	378.7	$Ha \times$ Å
L	Penalty for variation in x secn. strains	-150.4	-356.4	$Ha \times$ Å

Table 3.1: Material parameters for (9,6) and (10,10) SWNT

material parameters for the (10,10) SWNT have been obtained from the Tersoff-Brenner potential [33].

3.2 Equations of Equilibrium

Nine unknown field variables have been presented in the previous section: three variables corresponding to the centerline displacement **r**, three variables corresponding to rigid rotation of cross-section **R** and three for in-plane cross-sectional deformation $\underline{z}$. To solve for these variables, nine equations are needed. The first six euqations are the usual linear and the angular momentum balance equations as in the special Cosserat rod theory:

$$\begin{aligned} \mathbf{LMB} &: \mathbf{n}' + \mathbf{f} = \mathbf{0} \\ \mathbf{AMB} &: \mathbf{m}' + \mathbf{r}' \times \mathbf{n} + \mathbf{g} = \mathbf{0} \end{aligned} \tag{3.7}$$

Here $\mathbf{n} = \mathbf{R}\frac{\partial \Phi}{\partial \underline{\mathrm{v}}}$ and $\mathbf{m} = \mathbf{R}\frac{\partial \Phi}{\partial \underline{\mathrm{k}}}$ denote the internal contact force and the internal moment acting at a cross-section, while **f** and **g** denote the distributed force and the distributed couple per unit of undeformed length respectively, acting along

the length of rod. The last three equations were proposed in Kumar et al. [32] as:

$$\mathrm{Q}_1' - \mathrm{q}_1 + \mathrm{r}_1 = 0 \tag{3.8}$$

$$\mathrm{Q}_2' - \mathrm{q}_2 + \mathrm{r}_2 = 0 \tag{3.9}$$

$$\mathrm{Q}_3' - \mathrm{q}_3 + \mathrm{r}_3 = 0 \tag{3.10}$$

If one writes $\underline{\mathrm{Q}} = \begin{bmatrix} \mathrm{Q}_1 \\ \mathrm{Q}_2 \\ \mathrm{Q}_3 \end{bmatrix}$, $\underline{\mathrm{q}} = \begin{bmatrix} \mathrm{q}_1 \\ \mathrm{q}_2 \\ \mathrm{q}_3 \end{bmatrix}$ and $\underline{\mathrm{r}} = \begin{bmatrix} \mathrm{r}_1 \\ \mathrm{r}_2 \\ \mathrm{r}_3 \end{bmatrix}$, the three additional equations can be written in compact form as:

$$\begin{aligned} \underline{\mathrm{Q}}' - \underline{\mathrm{q}} + \underline{\mathrm{r}} &= \mathbf{0} \\ \text{or, } \left(\frac{\partial \Phi}{\partial \underline{\mathrm{z}}'}\right)' - \frac{\partial \Phi}{\partial \underline{\mathrm{z}}} + \underline{\mathrm{r}} &= \mathbf{0} \end{aligned} \tag{3.11}$$

Here, $Q_1 = \frac{\partial \Phi}{\partial a'}$, $Q_2 = \frac{\partial \Phi}{\partial b'}$ and $Q_3 = \frac{\partial \Phi}{\partial c'}$ are the conjugate forces associated with cross-sectional deformations a', b' and c'. Similarly, $q_1 = \frac{\partial \Phi}{\partial a}$, $q_2 = \frac{\partial \Phi}{\partial b}$ and $q_3 = \frac{\partial \Phi}{\partial c}$ are the conjugate forces associated with cross-sectional deformation parameters a, b and c. The distributed conjugate forces are:

$$\begin{aligned} \mathrm{r}_1 &= \mathbf{e}_1 \cdot \mathbf{R}^T \left[\int_{\partial\Omega} X_1 \mathbf{P}\boldsymbol{\nu} + \int_{\Omega} X_1 \rho_0 \mathbf{b} \right] \\ \mathrm{r}_2 &= \mathbf{e}_2 \cdot \mathbf{R}^T \left[\int_{\partial\Omega} X_2 \mathbf{P}\boldsymbol{\nu} + \int_{\Omega} X_2 \rho_0 \mathbf{b} \right] \\ \mathrm{r}_3 &= \mathbf{e}_2 \cdot \mathbf{R}^T \left[\int_{\partial\Omega} X_1 \mathbf{P}\boldsymbol{\nu} + \int_{\Omega} X_1 \rho_0 \mathbf{b} \right] + \mathbf{e}_1 \cdot \mathbf{R}^T \left[\int_{\partial\Omega} X_2 \mathbf{P}\boldsymbol{\nu} + \int_{\Omega} X_2 \rho_0 \mathbf{b} \right] \end{aligned} \tag{3.12}$$

Thus (3.7) and (3.11) together form a complete set of nine ordinary differential equations. The set of ODEs can be solved using a variational formulation. This approach is presented in the next section.

3.3 Variational Formulation to Solve the System of ODEs

In order to solve equations (3.7) and (3.11), a weak form of the equilibrium equations (which enables the unknowns to belong in the space C^1 compared with C^2 in strong form) was proposed by Kumar et al. [32].

The unknowns that need to be solved for are $\mathbf{r}(s)$, $\mathbf{R}(s)$ and z(s) in C^1. Now define $\boldsymbol{\theta}(s)$ as a vector directed along the axis of ratation of $\mathbf{R}(s)$. Accordingly, $\boldsymbol{\theta}(s)$ denotes the angle of rotation. Further, let $\boldsymbol{\Theta}(s)$ be a skew symmetric matrix whose axial vector is $\boldsymbol{\theta}(s)$. Then, $\mathbf{R}(s) = exp(\boldsymbol{\Theta}(s))$. Assuming absence of lateral traction or body force, one arrives at the following "spatial" weak form:

$$G \equiv \int_0^1 \mathbf{n}' \cdot \boldsymbol{\eta}_0 + (\mathbf{m}' + \mathbf{r}' \times \mathbf{n}) \cdot \boldsymbol{\psi} + \left(\underline{\mathrm{Q}}' - \underline{\mathrm{q}}\right) \cdot \boldsymbol{\lambda}\, ds \tag{3.13}$$

Here, $\boldsymbol{\eta}(s) \equiv (\boldsymbol{\eta}_0(s), \boldsymbol{\psi}(s), \boldsymbol{\lambda}(s))$ are the admissible test functions (arbitrarily smooth). Also, $\boldsymbol{\eta}_0$ and $\boldsymbol{\psi}$ correspond to smooth variations of $\mathbf{r}$ and $\boldsymbol{\theta}$ respectively, whereas $\boldsymbol{\lambda}$ corresponds to smooth varitaion in the cross-sectional strain measure $\underline{\mathrm{z}}$. These functions may vanish at the boundary. Then (3.13) is integrated by parts to get:

$$G \equiv \int_0^1 \left[\mathbf{n} \cdot (\boldsymbol{\eta}_0' - \boldsymbol{\psi} \times \mathbf{r}') + \mathbf{m} \cdot \boldsymbol{\psi}' + \underline{\mathrm{Q}} \cdot \boldsymbol{\lambda}' + \underline{\mathrm{q}} \cdot \boldsymbol{\lambda}\right] ds - \left(\mathbf{n} \cdot \boldsymbol{\eta}_0 + \mathbf{m} \cdot \boldsymbol{\psi} + \underline{\mathrm{Q}} \cdot \boldsymbol{\lambda}\right)\Big|_0^1 \tag{3.14}$$

The boundary terms $\left(\mathbf{n} \cdot \boldsymbol{\eta}_0 + \mathbf{m} \cdot \boldsymbol{\psi} + \underline{\mathrm{Q}} \cdot \boldsymbol{\lambda}\right)\Big|_0^1$ in the expression (3.14) will vanish for Dirichlet problems (or free boundary problems) as the admissible smooth test functions (or the stress resultants) vanish at the boundary in such cases. It should be noted that the boundary terms in the expression (3.14) could render DG, the linearized part of G (the tangent stiffness operator), non-symmetric in the case of non-conservative problems [31, 48].

In order to linearize the weak form, let $\boldsymbol{\phi}_\epsilon(s) = (\mathbf{r}(s)+\epsilon\triangle\mathbf{r}(s), \exp(\epsilon\triangle\boldsymbol{\theta}(s))\mathbf{R}(s), \underline{z}(s)+\epsilon\triangle\underline{z}(s))$ be the perturbed configuration of a rod about any configuration $\boldsymbol{\phi}(s) = \left(\mathbf{r}(s), \mathbf{R}(s), \underline{z}(s)\right)$. Hence, using Taylor's expansion:

$$G(\boldsymbol{\phi}_\epsilon, \boldsymbol{\eta}) = G(\boldsymbol{\phi}, \boldsymbol{\eta}) + \epsilon DG(\boldsymbol{\phi}, \boldsymbol{\eta})\left[\triangle\boldsymbol{\phi}\right] + o\left(|\epsilon\triangle\boldsymbol{\phi}|\right). \tag{3.15}$$

The discrete form of expression (3.15), obtained by the finite element procedure, is carried out in the following section. The static equilibria are obtained through Newton's iterative method. Below we show an expression for the tangent stiffness operator whose derivation follows along the lines of Simo & Vu-Quoc [48]. Following their notation [48], define:

$$\tilde{\mathbf{C}}_{(9\times9)} = \begin{bmatrix} \frac{\partial^2\Phi}{\partial\underline{v}^2} & \frac{\partial^2\Phi}{\partial\underline{v}\partial\underline{k}} & \frac{\partial^2\Phi}{\partial\underline{v}\partial\underline{z}'} \\ \frac{\partial^2\Phi}{\partial\underline{k}\partial\underline{v}} & \frac{\partial^2\Phi}{\partial\underline{k}^2} & \frac{\partial^2\Phi}{\partial\underline{k}\partial\underline{z}'} \\ \frac{\partial^2\Phi}{\partial\underline{z}'\partial\underline{v}} & \frac{\partial^2\Phi}{\partial\underline{z}'\partial\underline{k}} & \frac{\partial^2\Phi}{\partial\underline{z}'^2} \end{bmatrix}, \quad \Pi_{(6\times6)} = \begin{bmatrix} \mathbf{R} & \mathbf{0} \\ \mathbf{0} & \mathbf{R} \end{bmatrix}, \quad \mathbf{E}^T_{(6\times6)} = \begin{bmatrix} \mathbf{1}\frac{d}{ds} & \mathbf{r}'\times \\ \mathbf{0} & \mathbf{1}\frac{d}{ds} \end{bmatrix}$$

$$\mathbf{Cz}_{(9\times3)} = \begin{bmatrix} \frac{\partial^2\Phi}{\partial\underline{v}\partial\underline{z}} \\ \frac{\partial^2\Phi}{\partial\underline{k}\partial\underline{z}} \\ \frac{\partial^2\Phi}{\partial\underline{z}'\partial\underline{z}} \end{bmatrix}, \quad \mathbf{C}_{(12\times12)} = \begin{bmatrix} \tilde{\mathbf{C}} & \mathbf{Cz} \\ \mathbf{Cz}^T & \frac{\partial^2\Phi}{\partial\underline{z}^2} \end{bmatrix}$$

Thus:

$$\begin{aligned} DG(\boldsymbol{\phi}, \boldsymbol{\eta})\left[\triangle\boldsymbol{\phi}\right] \equiv \int_0^1 & \begin{bmatrix} \mathbf{E}\Pi & \mathbf{0}_{(6\times3)} & \mathbf{0}_{(6\times3)} \\ \mathbf{0}_{(3\times6)} & \mathbf{1}\frac{d}{ds} & \mathbf{1} \end{bmatrix} \mathbf{C} \begin{bmatrix} \mathbf{E}\Pi & \mathbf{0}_{(6\times3)} & \mathbf{0}_{(6\times3)} \\ \mathbf{0}_{(3\times6)} & \mathbf{1}\frac{d}{ds} & \mathbf{1} \end{bmatrix}^T \triangle\boldsymbol{\phi}\cdot\boldsymbol{\eta} \\ & + \begin{bmatrix} \mathbf{0} & -\mathbf{n}\times \\ \mathbf{0} & -\mathbf{m}\times \end{bmatrix} \begin{bmatrix} \triangle\mathbf{r}_0 \\ \triangle\boldsymbol{\theta}_0 \end{bmatrix} \cdot \mathbf{E}^T \begin{bmatrix} \boldsymbol{\eta_0} \\ \boldsymbol{\psi} \end{bmatrix} + (\mathbf{n}\times\triangle\mathbf{r}_0')\cdot\boldsymbol{\psi}\, ds \end{aligned} \tag{3.16}$$

The tangent stiffness operator (3.16) resembles structrually the one proposed by Simo and Vu-Quoc [48]. As a result, an analogous finite element method formulation can be carried out here.

3.4 Finite Element Formulation

In this section, a finite element formulation is presented based on the variational equations discussed in the prevous section. Details of the discretization and finite element arrays will be considered first. The updating procedure using the Newton-Raphson method is examined subsequently.

3.4.1 Discretization of the Domain

Consider a standard finite element discretizaion on the 1-D domain $[0, L] = \sum_{i=1}^{n} h_i$, where n is the the number of elements and $h_i = L/n$ denotes the typical length of each element. Accordingly, let $\Delta\boldsymbol{\phi}^h = (\Delta\mathbf{r}^h, \Delta\boldsymbol{\theta}^h, \Delta z^h)$ be the incremental field superposed onto the configuration Φ. The incremental field in terms of shape functions can be formulated as:

$$\begin{aligned}
\Delta\mathbf{r}^h(s) &= \sum_{i=1}^{2} N_i(s)\Delta\mathbf{r}_i(s), \\
\Delta\boldsymbol{\theta}^h(s) &= \sum_{i=1}^{2} N_i(s)\Delta\boldsymbol{\theta}_i(s), \\
\Delta z^h(s) &= \sum_{i=1}^{2} N_i(s)\Delta z_i(s)
\end{aligned} \tag{3.17}$$

where $N_i(s)$ denotes the linear shape function associated with node i, and $r_i(s), \theta_i(s)$ and $z_i(s)$ are the nodal incremental variables of the centerline position, rotation of cross-section and cross-sectional deformation at node i. In this paper, a rod element has two nodes. Linear shape functions are used here:

$$N_1 = \frac{h_i - s}{h_i}, \quad N_2 = \frac{s}{h_i} \tag{3.18}$$

3.4.2 Descretization of the Linearied Weak Form

Now consider the linearized weak form. The linear part of the weak form at the configuration $\boldsymbol{\phi}$ can be expressed as:

$$DG^h(\boldsymbol{\phi}^h, \boldsymbol{\eta}^h)[\Delta\boldsymbol{\phi}^h] = -\mathbf{P}^h(\boldsymbol{\phi}) \cdot \boldsymbol{\eta}^h \tag{3.19}$$

where $\mathbf{P}^h(\boldsymbol{\phi})$ denotes the unbalanced force vector in a typical element. Neglecting the body force, the unbalanced nodal force in a typical element has the following expression:

$$\mathbf{P}^h(\boldsymbol{\phi}) = \int O^h \begin{bmatrix} \mathbf{n}^h \\ \mathbf{m}^h \\ Q^h \\ q^h \end{bmatrix} ds \tag{3.20}$$

where O^h represents the discrete differential operater associated with node i. Assume that the spatial stress vector is $[\mathbf{m}^h, \mathbf{n}^h, Q^h, q^h]$. Substitution of (3.17) into the operator yields:

$$O^h = \begin{bmatrix} N_i'\mathbf{1} & \mathbf{0} & \mathbf{0} & \mathbf{0} \\ -N_i[\mathbf{r}'\times] & N_i'\mathbf{1} & \mathbf{0} & \mathbf{0} \\ \mathbf{0} & \mathbf{0} & N_i'\mathbf{1} & -\mathbf{1} \end{bmatrix} \tag{3.21}$$

This completes the computation of the local residual vector.

3.4.3 Computation of Tangent Stiffness Matrix

Now consider the discretized linearized weak form. Here, linear shape functions are used in the discretized linear parts of the weak form, as:

$$L[G^h(\boldsymbol{\phi}^h, \boldsymbol{\eta}^h)] = \boldsymbol{\eta}^h \cdot [\{\mathbf{S}^h(\boldsymbol{\phi}^h) + \mathbf{T}^h(\boldsymbol{\phi}^h)\}\Delta\boldsymbol{\phi}^h + \mathbf{P}^h(\boldsymbol{\phi})] \tag{3.22}$$

where $\mathbf{S}^h(\boldsymbol{\phi}^h)$ and $\mathbf{T}^h(\boldsymbol{\phi}^h)$ represent the element material stiffness matrix and the element geometric stiffness matrix, respectively. Now the shape functions in (3.17) can be incoporated into the expressions for the material and geometric stiffness matrices. One gets:

$$S^h_{ij} = \int \begin{bmatrix} \mathbf{E}^h_i \Pi & \mathbf{0}_{(6\times3)} & \mathbf{0}_{(6\times3)} \\ \mathbf{0}_{(3\times6)} & N_i' \mathbf{1} & N_i \mathbf{1} \end{bmatrix} \mathbf{C} \begin{bmatrix} \mathbf{E}^h_j \Pi & \mathbf{0}_{(6\times3)} & \mathbf{0}_{(6\times3)} \\ \mathbf{0}_{(3\times6)} & N_j' \mathbf{1} & N_j \mathbf{1} \end{bmatrix}^T ds \tag{3.23}$$

In this expression, $\mathbf{E}^h_i$ contains the discrete differential operators which are defined as:

$$\mathbf{E}^h_i = \begin{bmatrix} N_i' \mathbf{1} & \mathbf{0} \\ -N_i[\mathbf{r}'\times] & N_i' \mathbf{1} \end{bmatrix}. \tag{3.24}$$

and $\mathbf{C}$ is the elasticity tenor and defined as:

$$\mathbf{C}_{(12\times12)} = \begin{bmatrix} \tilde{\mathbf{C}} & \mathbf{Cz} \\ \mathbf{Cz}^T & \frac{\partial^2 \Phi}{\partial \underline{z}^2} \end{bmatrix}$$

The strain energy dessity Φ of a single walled carbon nanotube is defined in (3.6). The expression in (3.6) is used to calculate the elasticity tensor $\mathbf{C}$ as fol-

lows:

$$\mathbf{C} = \begin{bmatrix} \begin{bmatrix} C & 0 & 0 \\ 0 & C & 0 \\ 0 & 0 & D \end{bmatrix} & \begin{bmatrix} F & 0 & 0 \\ 0 & F & 0 \\ 0 & 0 & E \end{bmatrix} & & \begin{bmatrix} 0 & 0 & 0 \\ 0 & 0 & 0 \\ \frac{G}{2} & \frac{G}{2} & 0 \end{bmatrix} \\ \begin{bmatrix} F & 0 & 0 \\ 0 & F & 0 \\ 0 & 0 & E \end{bmatrix} & \begin{bmatrix} A & 0 & 0 \\ 0 & A & 0 \\ 0 & 0 & B \end{bmatrix} & \begin{bmatrix} \mathbf{0} \end{bmatrix} & \begin{bmatrix} 0 & 0 & 0 \\ 0 & 0 & 0 \\ \frac{H}{2} & \frac{H}{2} & 0 \end{bmatrix} \\ \begin{bmatrix} \mathbf{0} \end{bmatrix} & \begin{bmatrix} \mathbf{0} \end{bmatrix} & \begin{bmatrix} \frac{K}{4} & \frac{K}{4}+\frac{L}{2} & 0 \\ \frac{K}{4}+\frac{L}{2} & \frac{K}{4} & 0 \\ 0 & 0 & -L \end{bmatrix} & \begin{bmatrix} \mathbf{0} \end{bmatrix} \\ \begin{bmatrix} 0 & 0 & \frac{G}{2} \\ 0 & 0 & \frac{G}{2} \\ 0 & 0 & 0 \end{bmatrix} & \begin{bmatrix} 0 & 0 & \frac{H}{2} \\ 0 & 0 & \frac{H}{2} \\ 0 & 0 & 0 \end{bmatrix} & \begin{bmatrix} \mathbf{0} \end{bmatrix} & \begin{bmatrix} \frac{I}{4} & \frac{I}{4}+\frac{J}{2} & 0 \\ \frac{I}{4}+\frac{J}{2} & \frac{I}{4} & 0 \\ 0 & 0 & -J \end{bmatrix} \end{bmatrix}. \quad (3.25)$$

The geometric tangent stiffness is obtained by evaluating the geometric contribution of the tangent stiffness. The discrete form of the geometric tangent stiffness matrix has the form:

$$T_{ij}^{h} = \int \begin{bmatrix} \mathbf{0} & -[\mathbf{n}^{h}\times]^{h}N_{i}^{'}N_{j} \\ [\mathbf{n}^{h}\times]N_{i}N_{j}^{'} & -[\mathbf{m}\times]N_{i}^{'}N_{j} + [\mathbf{n}^{h}\otimes\mathbf{r}_{0}^{'} - (\mathbf{n}\cdot\mathbf{r}_{0}^{'})\mathbf{1}]N_{i}N_{j} \end{bmatrix} ds. \quad (3.26)$$

Here, $\mathbf{n}^{h}$ is a discretized version of $\mathbf{n}$, and $[(\cdot)\times]$ is a skew-symmertic matrix whose axial vector is $(\cdot)$. This expression of the geometric stiffness matrix has been proposed by Simo and Vu-Quoc [48].

3.4.4 Configuration Updating Algorithm

The updating procedure for the equilibrium configuration using a Newton-Raphson strategy is presented next. In a typical iterative method, assume the current configuration $\mathbf{\Phi}_n = (\mathbf{r}_n(s), \mathbf{R}_n(s), z_n(s))$ is obtained. Then solve the linearized weak form (3.19) for an incremental deformation $(\Delta\mathbf{r}, \Delta\boldsymbol{\theta}, \Delta z)$. Here, $\Delta\mathbf{r}$ is the increment of the deformation of the centerline, $\Delta\boldsymbol{\theta}$ is the increment of the axial vector of the skew-symetric tensor $\mathbf{\Theta}$ and Δz is the incremental deformation of the cross-section. An update procedure is given by the formulae:

$$\begin{aligned} \mathbf{r}_{n+1}(s) &= \mathbf{r}_n(s) + \Delta\mathbf{r}, \\ \mathbf{R}_{n+1}(s) &= exp[\mathbf{\Theta}(s)]\mathbf{R}_n(s), \\ z_{n+1}(s) &= z_n(s) + \Delta z(s) \end{aligned} \tag{3.27}$$

It should be noted that the exponential of a skew symmetric matrix $\exp[\mathbf{\Theta}(s)]$ is an orthogonal rotation matrix. This matrix can be calculated from the axial vector $\Delta\boldsymbol{\theta}$ using quaternions. Let $\mathbf{q} = q_0 + q_1\mathbf{e}_1 + q_2\mathbf{e}_2 + q_3\mathbf{e}_3$. Recall that quaternions can be expressed as:

$$\mathbf{q} = \cos(\frac{1}{2}\,||\Delta\boldsymbol{\theta}||) + \frac{\Delta\boldsymbol{\theta}}{||\Delta\boldsymbol{\theta}||}\sin(\frac{1}{2}\,||\Delta\boldsymbol{\theta}||). \tag{3.28}$$

Finally, $\exp[\mathbf{\Theta}(s)]$ can be expressed by the four quaternions as:

$$\exp[\mathbf{\Theta}(s)] = 2\begin{bmatrix} q_0^2 + q_1^2 - \frac{1}{2} & q_1q_2 - q_3q_0 & q_1q_3 + q_2q_0 \\ q_2q_1 + q_3q_0 & q_0^2 + q_2^2 - \frac{1}{2} & q_2q_3 - q_1q_0 \\ q_3q_1 - q_2q_0 & q_3q_2 + q_1q_0 & q_0^2 + q_3^2 - \frac{1}{2} \end{bmatrix} \tag{3.29}$$

The iterations terminate when (3.19) is satisfied within a given precision.

3.5 Numerical Examples

In this section, several numerical examples, that illustrate the performance of the formulation above, are presented using the finite element solver. The first example investigates the coupling between extension and twist, extention and cross-sectional deformation and twist and cross-sectional deformation of a 9×6 chiral SWNT. The primary objective of this example is to show that the model above has the capability to model a chiral SWNT. The effect of chirality is often neglected in other continuum models of SWNTs.

It is noted that the parameters listed in Table 3.1 are used for the (9,6) chiral SWNT simulations. The partial set of parameters (from Table 3.1), that are active for these coupled axial extension-twist-cross-sectional deformation mode simulations, have been obtained from the Tersoff-Brenner potential in a consistant manner [33].

The next example is concerned with the buckling behavior of a (10,10) armchair SWNT. Its material parameters are also listed in Table 3.1. The effect of chirality is dominant only in coupled extension-twist-cross-sectional stretch modes, so the (9,6) SWNT is used for this example. However, the bending modulus does not change a lot when a nanotube is twisted even by 10 percent [33]. Hence, an armchair (10,10) SWNT is used for buckling analysis so that buckling can be analyzed independent of chiral effects (if any).

3.5.1 Coupling between Extension, Twist and Cross-sectional Deformation Modes

This example is devised to show the coupling of the aformentioned deformation modes for a (9,6) chiral SWNT. The coupling between extension and twist of a SWNT is has been reported in Chandraseker and Mukherjee [8]. Here, a straight (9,6) chiral SWNT with diameter 1nm and length 10nm is clamped at one end against both rotation and translation but change of its radius is allowed, while the other end is free from constraint and with prescribed force and moment boundary conditions. Three different cases are investigated here. In the first case, the SWNT is axially stretched from a relaxed configuration. The top two curves in Fig. 3.2 show the induced cross-sectional deformation due to extension and induced twist due to extension. Here r denotes the radius of SWNT and ϵ denotes the axial strain. In the second and third cases, the SWNT is subjected to twist from a relaxed configuration. The middle two curves in Fig. 3.2 describe the induced cross-sectional deformation due to twist in opposite directions. Finally, the bottom two curves describe the induced extension and compression due to applied twist in opposite directions.

It is seen from Fig. 3.2 that the usual Poisson effect (shinkage of the cross-section of a SWNT induced by applied axial extension) is significant with an average value of Poisson's ratio around 0.3. Fig. 3.2 also shows that the other couplings (extension-twist and twist-cross-sectional deformation) are present, although rather weak.

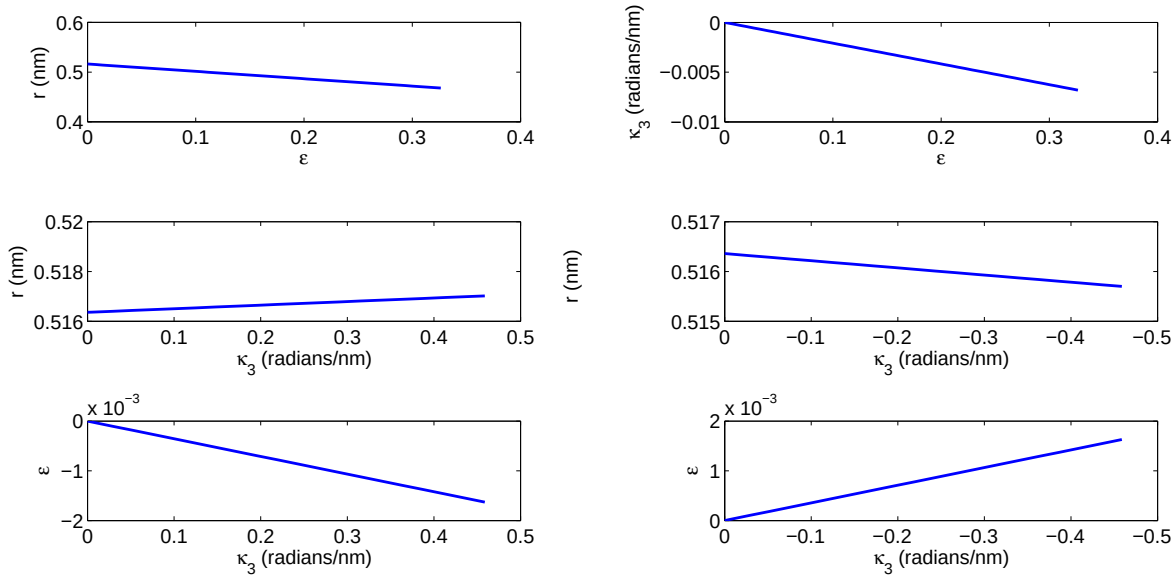

Figure 3.2: Coupling between extension, twist and cross-sectional deformation of an 9×6 chiral SWNT

3.5.2 Euler Buckling of a (10,10) SWCNT

This section presents a numerical example corresponding to Euler buckling of a (10,10) nanotube when it is compressed. The nanotube contains 2000 carbon atoms and its radius is 0.69 nm. The boundary conditions at the two ends are prescribed as in the equations (3.30) and (3.31).

$$\begin{aligned} \mathrm{r}_\alpha(-1) = 0, \alpha = 1,2, \quad \mathrm{r}_3(-1) &= (-1+\lambda)\, L/2 \\ \mathbf{R}(-1) &= \mathbf{I} \\ a(-1) = b(-1) &= 1.0 \\ c(-1) &= 0 \end{aligned} \tag{3.30}$$

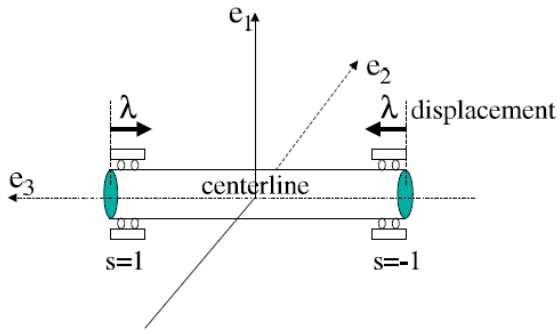

Figure 3.3: A straight rod in the straight state reference configuration representing a naotube: λ denotes the compressive strain

$$
\begin{aligned}
& \mathrm{r}_\alpha(1) = 0, \alpha = 1, 2, \quad \mathrm{r}_3(1) = (1 - \lambda) L \\
& \mathbf{R}(1) = \mathbf{I} \\
& a(1) = b(1) = 1.0 \\
& c(1) = 0
\end{aligned}
\tag{3.31}
$$

The two ends are fully clamped. The axial displacements of the two end points are prescribed through the parameter λ as shown in Fig. 3.3.

The twelve material parameteres of this nanotube were obtained using the second generation Tersoff-brenner potential [33] and are shown in Table 3.1. These material parameters satisfy all the inequality constraints for this nanotube to be materially stable [31]. It may also be noted from Table 3.1 that the coupling parameters E, F and H are all zero since the nanotube is not chiral.

Fig. 3.4 shows the buckling load for this nanotube as a function of its length. The buckling load in the figure has been normalized by the Euler buckling

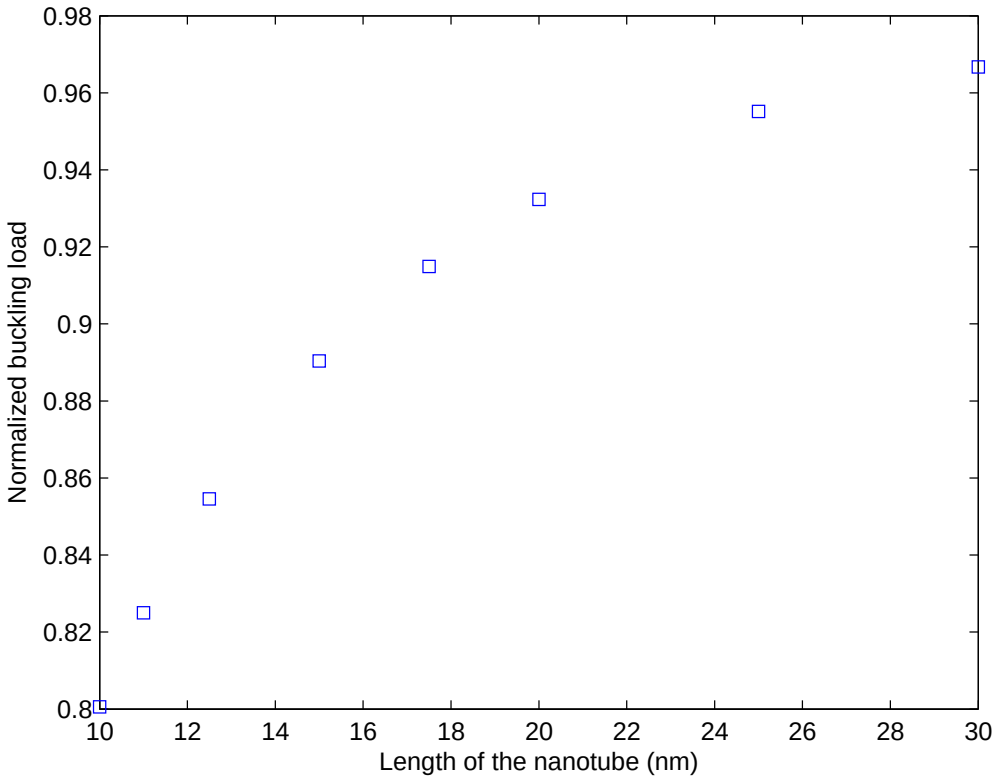

Figure 3.4: Normalized buckling load of a (10,10) nanotube as its length increases

load formula for clamped-clamped boundary conditions. It is observed that as the length of the nanotube increases, the nanotube starts behaving more like a Euler-Bernouli rod and its stretching becomes insignificant. Fig. 3.5 shows the bifurcation diagram for compression of a (10,10) nanotube 12.5 nm long. It plots the mid-point displacement of the nanotube on the y-axis. It can be observed that after a certain critical compression (7.7%), the straight state solution becomes unstable while a stable buckled configuration emerges. Fig. 3.6 shows how the axial force (copmpressive) varies as compression is increased. The compressive force in the figure has been normalized by the buckling load of the nanotube. Interestingly, after critical compression, the compressive axial

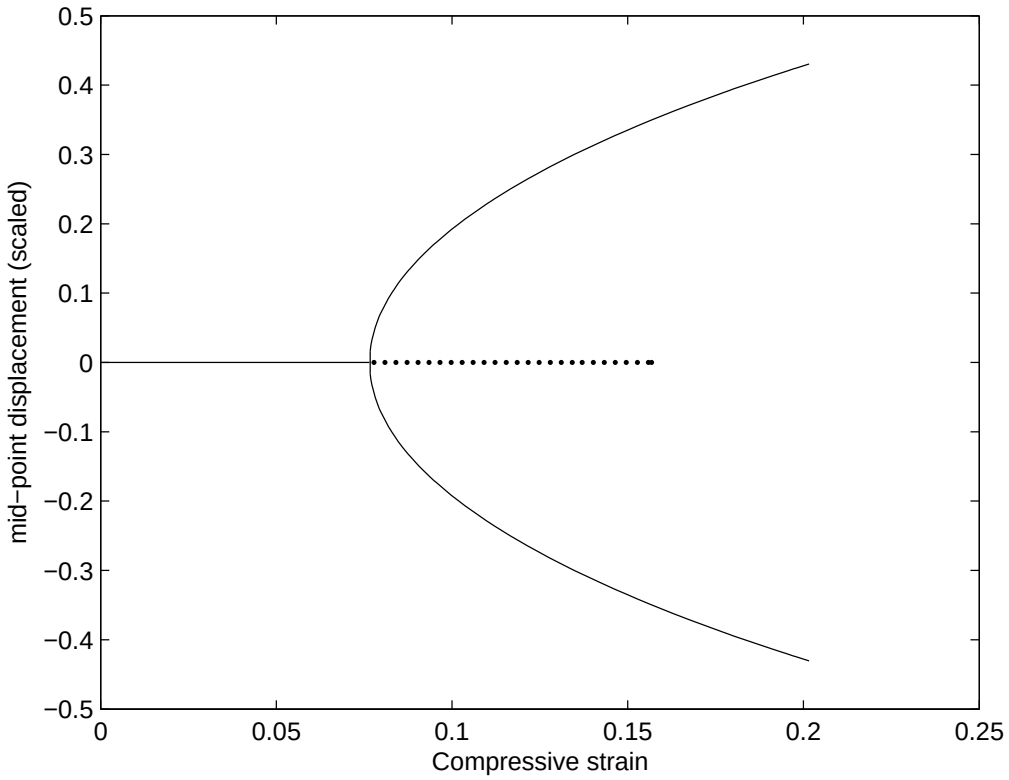

Figure 3.5: Bifurcation diagram of a (10,10) nanotube: Y-axis plots mid-point displacement

force in the buckled configuration does not change much. This fact suggests that the nanotube is releasing its extra compressive enenrgy by bending itself.

The next figures show how the radius of the nanotube is affected by compression. Fig. 3.7 shows the radius of a nanotube as a function of its length at 7.2% compression (just before buckling). It is seen that there is a small transition zone in which the radius of the nanotube changes abruptly and finally settles to a fixed value. More interestingly, Fig. 3.8 shows the same radius in the buckled configuration of a nanotube. Now the lateral surface of the nanotube becomes wavy when it buckles. A typical buckled configuration of this

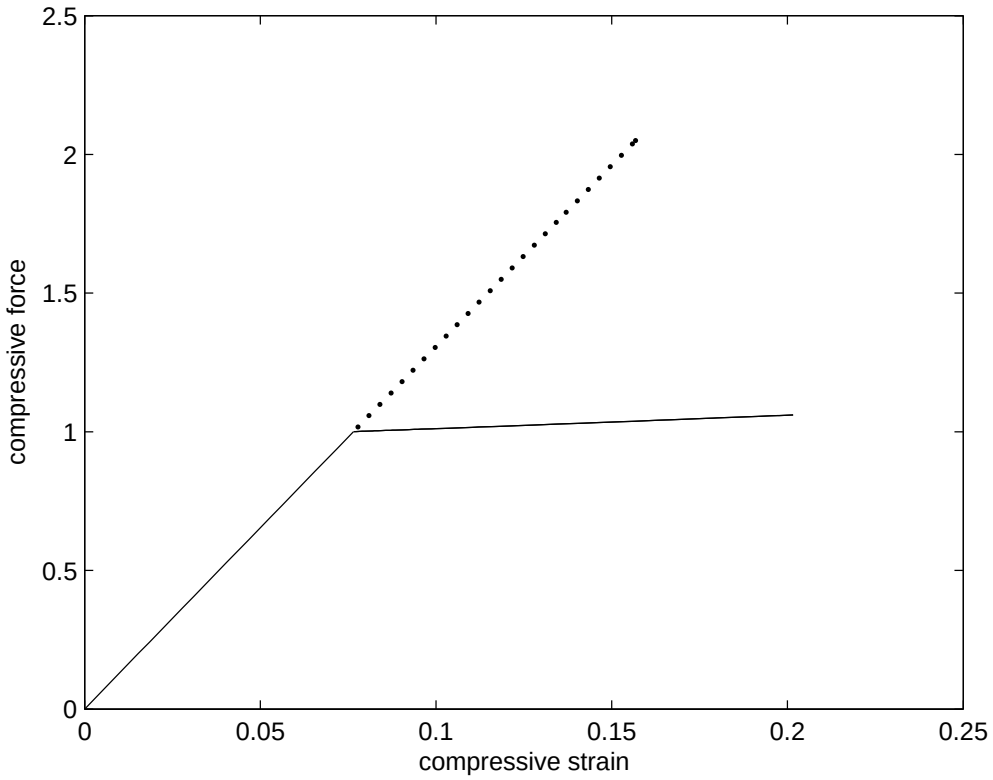

Figure 3.6: Normalized axial force (compressive) in a nanotube as it is compressed

nanotube is shown in Fig. 3.9.

3.6 Concluding Remarks

An atomistic continuum model, based on an extended Cosserat rod theory, for mechanical deformation of a SWNT, has been proposed recently[32]. The present paper carries out a FEM implementation of this model. Geometric non-

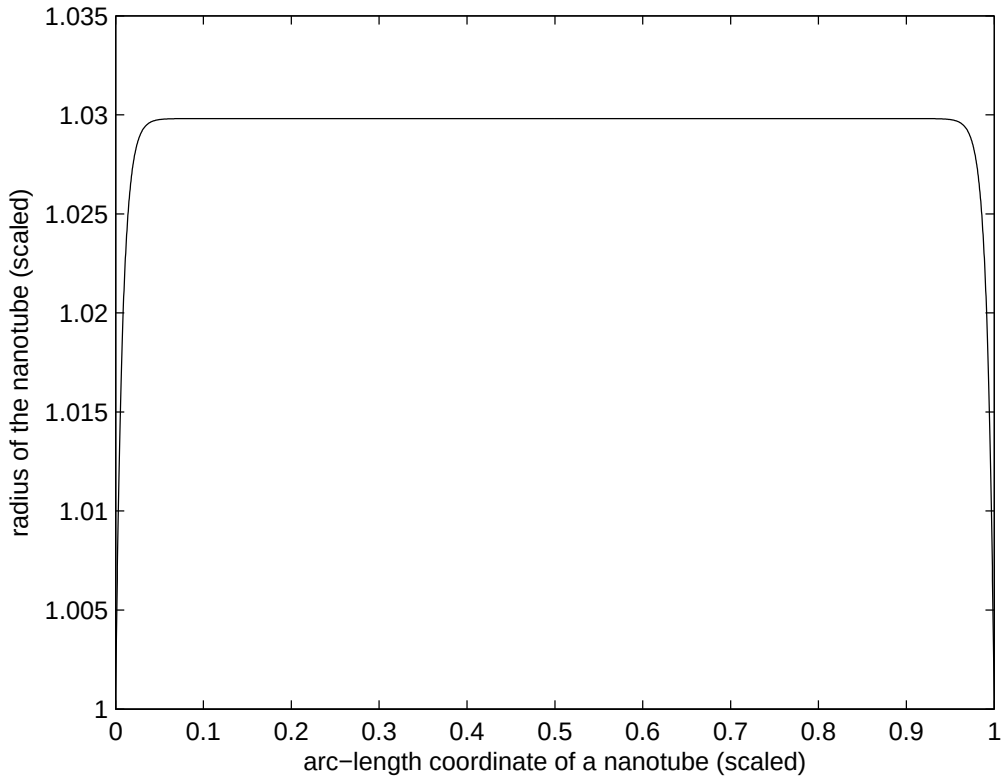

Figure 3.7: Radius of the nanotube in the straight state configuration

linearity is included in the FEM implementation. Two kinds of problems are considered in the numerical examples - coupling of extension, twist and cross-sectional deformation of a (9,6) chiral SWNT and Euler buckling of a (10,10) armchair SWNT.

An interesting problem is the dependence of material properties of a SWNT on a subset of these parameters, together with the chirality of the SWNT. This is a subject of ongoing work.

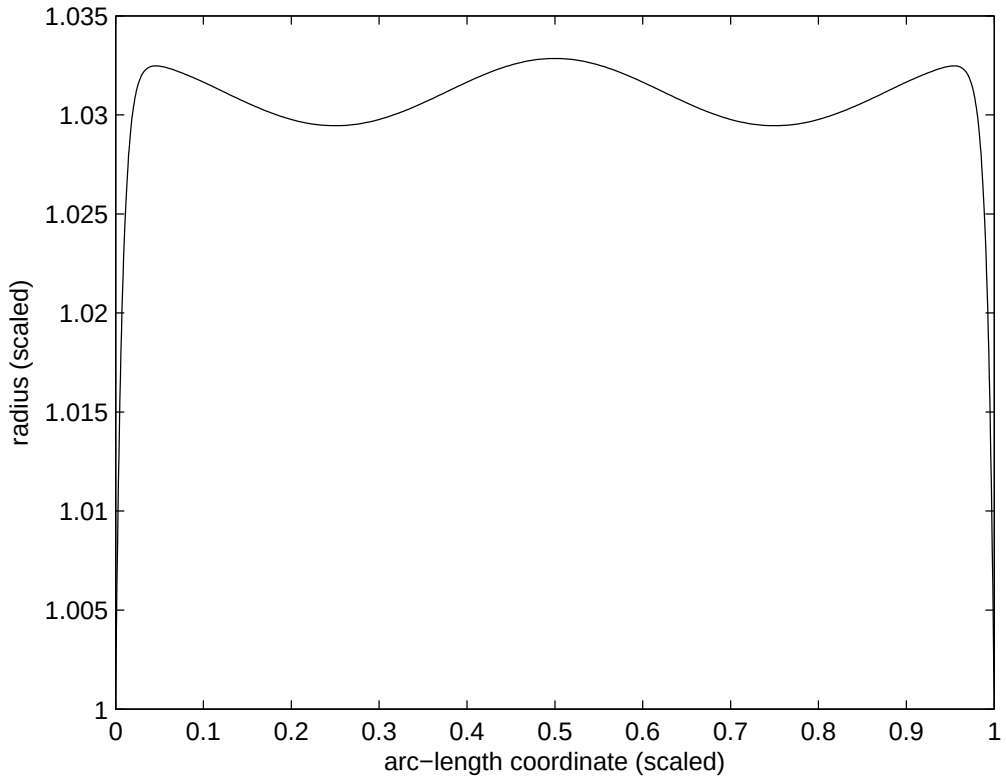

Figure 3.8: Radius of the nanotube in the buckled configuration: applied compressive strain is 15 %.

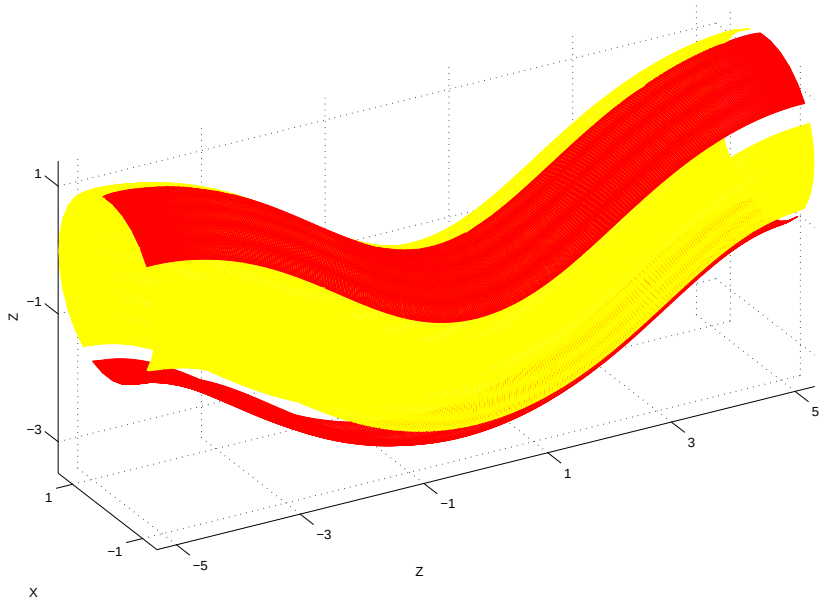

Figure 3.9: Buckled configuration of a nanotube at 15% applied compressive strain

CHAPTER 4

A CLASS OF REDUCED ELASTIC MODULI FOR THE ROD MODEL AND CONNECTION BETWEEN SWNTS WITH DIFFERENT CHIRALITIES

4.1 Introduction and Outline

The aformentioned rod model has a disadvantage that when modeling a SWNT, rod parameters need to be found on a case by case basis. This disadvatage limits the application of this rod model for SWNTs. In the present chapter, a class of reduced elastic moduli, based on the aformentioned twelve rod parameters, are derived for both an isotropic material and a transversly isotropic material. The approach is based on exploration of material symmetry. In the case of an isotropic material, the twelve rod parameters can be reduced to only two Lame's constants and areas of moments of inertia which are related to the geometry of a rod's cross-section. Carbon nanotubes are known be anisotropic. The type of a SWNT is determined by its chirality. The atomistic arrangement of a SWNT can be viewed as comprising a primary helical direction. The mechanical properties of a SWNT has been reported to be significantly affected by the chirality from both experiemtal studies and atomistic simulations. In the previous chapter, the (10,10) SWNT and (9,6) SWNT are described by different rod parameters. In this chapter, we will discuss the relationship between rod parameters and chirality of a SWNT. This is done primarily by exploring the material symmetry and constitutive relation of transversly isotropic materials with five material parameters. Explicit expression are presented for the twelve rod parameters in terms of the five material parameters, the chirality angle and the geometry of its cross-section. This is a unified approach to describe all types of SWNTs. It

is noted for this model that material symmetry is based on continuum mechanics. As a result, certain adjustments of parameters may be needed for describing SWNTs, which are atomistic structures. For example, in Chapter 2, the bending stiffness of a SWNT was found to be around $\frac{EI}{60}$ which can not be explained by continumm mechanics. More experimental efforts will be needed to finally determine this quantity.

The outline of this chapter is as follows. In Section 3.2, the rod parameters are derived based on the constitutive law for an isotropic material. In Section 3.3, the rod parameters for a SWNT are derived using the transversly isotropic assumption. In Section 3.4, the special case of armchair SWNT is discussed. Section 3.5 concludes this Chapter.

4.2 A Class of Reduced Elastic Moduli of Isotropic Rod Model

Simo and Vu-Quoc [49] succesfully reduced the elastic moduli of a special type of Cosserat rod model, including cross-section warping by exploiting material symmetry. This section is motivated by Simo's approach and a set of reduced moduli of the Cosserat rod model used in this dissertation are derived.

The goal is to obtain the nine Cosserat rod parameters A, B, B, D, G, I, J, K, L, in terms of the lame parameters and the geometry of the cross-section of an isotropic rod.
The deformation gradient can be written as:

$$\mathbf{F} = \mathbf{R}\left[\underline{v} \otimes \mathbf{e}_3 + X_\alpha(\mathbf{R}'\mathbf{U} + \mathbf{R}\mathbf{U}')\mathbf{e}_\alpha \otimes \mathbf{e}_3 + \mathbf{R}\mathbf{U}\mathbf{e}_\alpha \otimes \mathbf{e}_\alpha\right] \tag{4.1}$$

Here, $\underline{v} = \mathbf{R}^T\mathbf{r}'$ is a 3-vector, the first two components of which represent shear while the third component represents axial stretch, $\mathbf{K} = \mathbf{R}^T\mathbf{R}'$ is a skew symmetric matrix whose axial vector is a 3-vector, the first two components of which represent components of local curvature while the third component represents twist. $\mathbf{U}$ is defined in (3.3). Let $\mathbf{H}$ be a rank-two material tensor defined as $\mathbf{H} = \mathbf{R}^T\mathbf{F} - \mathbf{1}$. We have

$$\mathbf{H} = \underline{v} \otimes \mathbf{e}_3 + X_\alpha(\mathbf{R}'\mathbf{U} + \mathbf{R}\mathbf{U}')\mathbf{e}_\alpha \otimes \mathbf{e}_3 + \mathbf{R}\mathbf{U}\mathbf{e}_\alpha \otimes \mathbf{e}_\alpha - \mathbf{1} \tag{4.2}$$

Next, we define the symmetric part of $\mathbf{H}$ as $\mathbf{H}^s = \frac{1}{2}\left[\mathbf{H} + \mathbf{H}^T\right]$. As for small strains, the following constitutive equation is valid:

$$\Sigma_{\alpha\beta} = \left[\lambda\sigma_{\alpha\beta}\sigma_{\rho\theta} + 2\bar{G}\sigma_{\alpha\rho}\sigma_{\beta\theta}\right] H^s_{\rho\theta} \tag{4.3}$$

.

Here, λ and $\bar{G}$ denote the Lame's constants. As a derivation in elasticity, assume that $\Sigma_{\alpha 3} = 2\bar{G}H^s_{\alpha 3}$ and $\Sigma_{33} = \bar{E}H^s_{33} + \lambda H^s_{\alpha\alpha}$, where $\bar{G}$ denotes the shear modulus and $\bar{E}$ denotes the Young's modulus.

The internal contact force $\mathbf{N}$ can be found as follows:

$$\begin{aligned}
\mathbf{N} &= \mathbf{R}^T \int_\Omega \mathbf{P}\mathbf{e}_e d\Omega = \int_\Omega \Sigma_{i3}\mathbf{e}_i d\Omega \\
&= \int_\Omega \bar{G}\nu_\alpha \mathbf{e}_\alpha d\Omega + \int_\Omega (\lambda + 2\bar{G})(\nu_3 - 1)\,\mathbf{e}_3 d\Omega + \int_\Omega 2\lambda\left(\frac{a+b}{2} - 1\right)\mathbf{e}_3 d\Omega \\
&= \bar{G}\bar{A}\nu_\alpha \mathbf{e}_\alpha + (\lambda + 2\bar{G})\bar{A}(\nu_3 - 1)\mathbf{e}_3 + 2\lambda\bar{A}\left(\frac{a+b}{2} - 1\right)\mathbf{e}_3
\end{aligned} \tag{4.4}$$

Here $\bar{A}$ denotes the area of cross section of the rod.

In our isotropic rod model with nine parameters, the internal contact force can be derived from the strain energy expression as:

$$\mathbf{N} = \frac{\partial \Phi}{\partial \nu_i}\mathbf{e}_i = C\nu_\alpha \mathbf{e}_\alpha + D\left(\nu_3 - 1\right)\mathbf{e}_3 + G\left(\frac{a+b}{2} - 1\right)\mathbf{e}_3 \tag{4.5}$$

Comparing (4.4) with (4.26), the rod parameters C, D and C can be expressed in term of λ, $\bar{G}$ and $\bar{A}$ as follows:

$$\begin{aligned} C &= \bar{G}\bar{A} \\ D &= \left(\lambda + 2\bar{G}\right)\bar{A} \\ G &= 2\lambda\bar{A} \end{aligned} \tag{4.6}$$

Similarly, the internal contact moment $\mathbf{M}$ can be expressed as:

$$\begin{aligned} \mathbf{M} &= \mathbf{R}^T \int_\Omega X_\alpha \mathbf{R}\mathbf{U}\mathbf{e}_\alpha \times (\Sigma_{i3}\mathbf{e}_i)\, d\Omega \\ &= \int_\Omega \left(\lambda + 2\bar{G}\right) X_\alpha^2 \kappa_\alpha d\Omega + \int_\Omega \bar{G}(X_1^2 + X_2^2)\kappa_3 d\Omega \\ &= (\lambda + 2\bar{G})\bar{I}\kappa_\alpha \mathbf{e}_\alpha + \bar{G}\bar{J}\kappa_3 \mathbf{e}_3 \end{aligned} \tag{4.7}$$

Here, $\bar{I}$ is the moment of area and $\bar{J}$ denotes the polar moment of inertia. The internal contact moment can be obtained from the energy expression as:

$$\mathbf{M} = \frac{\partial \Phi}{\partial \kappa_i}\mathbf{e}_i = A\kappa_\alpha \mathbf{e}_\alpha + B\kappa_3 \mathbf{e}_3 \tag{4.8}$$

Thus, the bending and twisting moduli can be found as $A = (\lambda + 2\bar{G})\bar{I}$ and $B = \bar{G}\bar{J}$.

Next, we will derive the other moduli from the internal conjugate force expression:

$$Q_1 = \int_\Omega X_1 \mathbf{e}_1 \cdot \Sigma_{i3}\mathbf{e}_i d\Omega = \bar{G}\bar{I}a' \tag{4.9}$$

Here, Q_1 denotes the internal force conjugated to $a^{'}$. From the energy expression we also obtain:

$$Q_1 = \frac{\partial \Phi}{\partial a^{'}} = K\left(\frac{a^{'} + b^{'}}{2}\right) + \frac{L}{2}b^{'} \tag{4.10}$$

. Comparing the two expressions, K and L could be written as:

$$K = 4\bar{G}\bar{I}, \quad L = -2\bar{G}\bar{I} \tag{4.11}$$

The last three rod parameters can be derived from the internal force conjugated to a. Let q_1 be the conjugate force. Then, we have the following expression:

$$\begin{aligned} q_1 &= -\mathbf{e}_1 \cdot \kappa \times \mathbf{R}^T \int_\Omega X_1 \mathbf{P}\mathbf{e}_3 \, d\Omega + \int_\Omega \mathbf{e}_1 \cdot (\mathbf{R}^T \mathbf{P}\mathbf{e}_1) d\Omega \\ &= \left(\lambda + 2\bar{G}\right)\bar{A}\,(a-1) + \lambda\bar{A}\,(b-1) + \lambda\bar{A}\,(\nu_3 - 1) \end{aligned} \tag{4.12}$$

.

The expression of q_1 can also be obtained from strain energy equation as:

$$q_1 = \frac{\partial \Phi}{\partial a} = I\,(a-1) + I\,(b-1) + \frac{J}{2}\,(b-1) + \frac{G}{2}\,(\nu_3 - 1) \tag{4.13}$$

.

Finally, we obtain the last two rod modulus by comparing the two expressions of q_1 as:

$$I = 4\left(\lambda + 2\bar{G}\right)\bar{A}, \quad J = -4\bar{G}\bar{A} \tag{4.14}$$

It should be noted that these results are consistant with Chapter 2 except that the bending modulus was independent but now is based on beam theory.

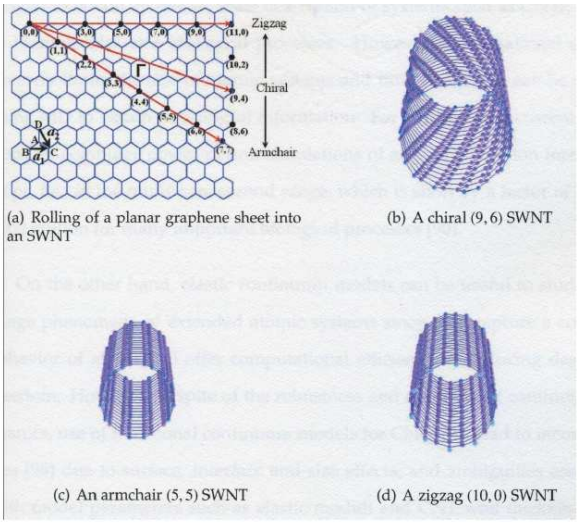

Figure 4.1: Different types of SWNT

4.3 A Class of Reduced Elastic Moduli for a Hemitropic Rod Model for a Chiral SWNT

SWNTs are classified as Zigzag, Armchair or chiral SWNT depending on the helical direction of the lattice (see Fig. 4.1). A chiral SWNT is the most general form of a SWNT since zigzag and armchair SWNT can be treated as a 0 degree and 90 degree chiral SWNT, respectively. A chiral SWNT is modeled in this work by a chiral rod model with twelve moduli. In this Chapter, we further explore the material symmetry of a SWNT to simplify the rod parameters. The hyperelastic transversly isotropic material symmetry is combined with a rod model to characterize the chirality of a SWNT. Specifically, we assume that the symmetry plane of a transversely isotropic material is perpendicular to the helical direction which is related to the chirality of a SWNT.

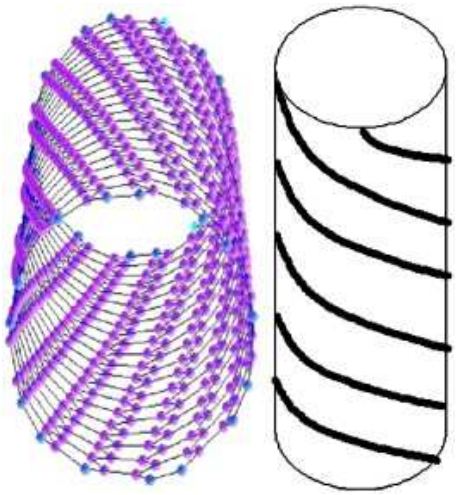

Figure 4.2: A Chiral SWNT in relaxed configuration

4.3.1 Transversely Isotropic Material Symmetry

A material is said to be orthotropic if it is characterized by symmetry with respect to three mutually orthogonal planes, reflection from which leaves material properties unchanged. The axes normal to these planes are called principal material directions. Transversely isotropic material symmetry is a special case of orthotropic material symmetery. In this case, all directions orthogonal to the principal material directions become equivalent. In this work, the principal material direction for a chiral SWNT can be described as the helical direction of the graphene latice. Let $\mathbf{l}_i \cdot \mathbf{l}_j = \delta_{ij}\,(i, j = 1, 2, 3)$ be the unit base vectors in the principal material directions. The structual tensors are defined as:

$$\mathbf{L}_i = \mathbf{l}_i \otimes \mathbf{l}_i, \quad i = 1, 2, 3. \tag{4.15}$$

Next, we will derive the mathmatical expressions for the principal material direction for a chiral SWNT. For a chiral SWNT in a relaxed configuration in Fig.

4.2, let $\mathbf{r}(s)$ be the position of a helix with respect to the rod coordinate s. Now, $\mathbf{r}(s)$ has the following form:

$$\mathbf{r}(s) = s\mathbf{e}_3 + X_\alpha \Theta_0 s\,(\mathbf{e}_3 \times \mathbf{e}_\alpha)\,. \tag{4.16}$$

In the expression above, Θ_0 is related to the chirality angle of a chiral SWNT. Θ_0 is the angle of rotation of the helix per unit length along the SWNT. This is:

$$\Theta_0 = \frac{\sqrt{3}(n-m)}{3c(m+n)} \tag{4.17}$$

Here, c denotes the radius of the SWNT. The direction of the helix of a SWNT can be found by taking the dirivative of the position vector as:

$$\mathbf{r}^{'} = \mathbf{e}_3 + \Theta_0 X_1 \mathbf{e}_2 - \Theta_0 X_2 \mathbf{e}_1. \tag{4.18}$$

Then the unit vector at the prime material direction $\mathbf{l}_1$ could be derived from $\mathbf{r}^{'}$ as

$$\mathbf{l}_1 = \frac{1}{\sqrt{1 + \Theta_0^2 X_1^2 + \Theta_0^2 X_2^2}}\,(\mathbf{e}_3 + \Theta_0 X_1 \mathbf{e}_2 - \Theta_0 X_2 \mathbf{e}_1)\,. \tag{4.19}$$

The structual tensors for transversely isotropic material can be expressed in this case by

$$\mathbf{L}_1 = \mathbf{l}_1 \otimes \mathbf{l}_1, \quad \mathbf{L}_2 = \mathbf{L}_3 = \frac{1}{2}\,(\mathbf{I} - \mathbf{l}_1 \otimes \mathbf{l}_1)\,, \tag{4.20}$$

where $\mathbf{I}$ denotes the second order identity tensor.

Next, we use the St. Venant-Kirchhoff model to represent the hyperelastic formulation of the transversely isotropic material. In this model, the constitutive relations can be written as:

$$\mathbf{\Sigma} = \sum_{i,j}^{3} a_{ij}\, tr\,(\mathbf{E}\mathbf{L}_i)\,\mathbf{L}_j + \sum_{i,j\neq i}^{3} 2G_{ij}\mathbf{L}_i\mathbf{E}\mathbf{L}_j. \tag{4.21}$$

Here, **E** denotes the Green strain tensor. It can be proved [49] that for small strain **E** is equavalent to **H**. In the expression of the stress tensor, the material constants are expressed by

$$\begin{aligned} &a_{ii} = \bar{E}_i \frac{1 - \bar{\nu}_{jk}\bar{\nu}_{kj}}{\Delta}, \quad a_{ij} = a_{ji} = \bar{E}_i \frac{\bar{\nu}_{ij} + \bar{\nu}_{kj}\bar{\nu}_{ik}}{\Delta}, \quad i \neq j \neq k \neq i, \quad i, j = 1, 2, 3 \\ &\Delta = 1 - \bar{\nu}_{12}\bar{\nu}_{21} - \bar{\nu}_{23}\bar{\nu}_{32} - 2\bar{\nu}_{21}\bar{\nu}_{32}\bar{\nu}_{13}. \end{aligned} \tag{4.22}$$

The St. Venant-Kirchhoff model contains the following material constants:

$$\begin{aligned} &\bar{E}_i (i = 1, 2, 3): \qquad Young's \quad moduli, \\ &\bar{G}_{ij} = \bar{G}_{ji} (i \neq j \neq 1, 2, 3): \qquad shear \quad moduli, \\ &\bar{\nu}_{ij} = \bar{\nu}_{ji} \frac{E_j}{E_i} (i \neq j \neq 1, 2, 3): \qquad Poisson's \quad ratios \end{aligned} \tag{4.23}$$

As for transversely isotropic material symmetry, all directions that are orthogonal to the principal material direction should be equivalent. The following relations are valid:

$$\bar{E}_3 = \bar{E}_2, \quad \bar{\nu}_{12} = \bar{\nu}_{13} \left(\bar{\nu}_{21} = \bar{\nu}_{31}\right), \quad \bar{G}_{21} = \bar{G}_{31}, \quad \bar{G}_{23} = \frac{\bar{E}_2}{2\left(1 + \bar{\nu}_{23}\right)}. \tag{4.24}$$

Here, because of the material symmetry, five independent material constant could be defined as

$$\begin{aligned} &\bar{E}_1, \quad \bar{E}_2: \qquad Young's \quad moduli, \\ &\bar{G} = \bar{G}_{12} = \bar{G}_{13}: \qquad shear \quad moduli, \\ &\bar{\nu}_1 = \bar{\nu}_{12}, \quad \bar{\nu}_2 = \bar{\nu}_{23}: \qquad Poisson's \quad ratios \end{aligned} \tag{4.25}$$

4.3.2 Rod Parameters in Term of Material Parameters and Chirality Angle

In a hemitropic rod model for a chiral SWNT with twelve parameters, the internal contact force can be derived from its strain energy expression as:

$$\mathbf{N} = \frac{\partial \Phi}{\partial \nu_i}\mathbf{e}_i = C\nu_\alpha \mathbf{e}_\alpha + D\left(\nu_3 - 1\right)\mathbf{e}_3 + E\kappa_3 \mathbf{e}_3 + F\kappa_\alpha \mathbf{e}_\alpha + G\left(\frac{a+b}{2} - 1\right)\mathbf{e}_3 \tag{4.26}$$

The internal contact force could also be derived from constitutive equations as

$$\mathbf{N} = \int_\Omega \Sigma_{13}\mathbf{e}_1 d\Omega + \int_\Omega \Sigma_{23}\mathbf{e}_2 d\Omega + \int_\Omega \Sigma_{33}\mathbf{e}_3 d\Omega. \tag{4.27}$$

Using expression in (4.21), the rod parameters: C,D,E,F,G can be found in the following form:

$$\begin{aligned} C = \int_\Omega & \frac{1}{\left(X_1^2 + X_2^2\right)\left(1 + \Theta_0^2 X_1^2 + \Theta_0^2 X_2^2\right)^2}\left(a_{11}\Theta_0^2 X_2^4 - a_{13}\Theta_0^2 X_2^4 - a_{31}\Theta_0^2 X_2^4\right. \\ & + a_{33}\Theta_0^2 X_2^4 + G_{21}X_1^2 + G_{31}X_2^2 + a_{11}\Theta_0^2 X_2^2 X_1^2 + a_{33}\Theta_0^2 X_2^2 X_1^2 - G_{13}\Theta_0^2 X_2^4 \\ & + G_{21}\Theta_0^2 X_2^4 + G_{23}\Theta_0^2 X_2^4 - G_{31}\Theta_0^2 X_2^4 + G_{13}\Theta_0^4 X_2^6 - a_{31}\Theta_0^2 X_2^2 X_1^2 - a_{13}\Theta_0^2 X_2^2 X_1^2 \\ & + 2G_{13}\Theta_0^4 X_2^4 X_1^2 + G_{13}\Theta_0^4 X_2^2 X_1^4 + G_{21}\Theta_0^2 X_2^2 X_1^2 + G_{23}\Theta_0^2 X_2^2 X_1^2 + 2G_{23}\Theta_0^4 X_2^2 X_1^4 \\ & \left. + G_{23}\Theta_0^4 X_2^2 X_1^4 - G_{31}\Theta_0^2 X_2^2 X_1^2 - G_{13}\Theta_0^2 X_2^2 X_1^2\right) d\Omega \end{aligned} \tag{4.28}$$

$$\begin{aligned} D = \int_\Omega & \frac{1}{\left(1 + \Theta_0^2 X_1^2 + \Theta_0^2 X_2^2\right)^2}\left(a_{33}X_2^4\Theta_0^4 + a_{33}X_1^4\Theta_0^4 + a_{31}X_2^2\Theta_0^2 + a_{31}X_1^2\Theta_0^2\right. \\ & + 2a_{33}X_1^2 X_2^2\Theta_0^4 + 2G_{13}X_2^2\Theta_0^2 + 2G_{13}X_1^2\Theta_0^2 + 2G_{31}X_2^2\Theta_0^2 + 2G_{31}X_1^2\Theta_0^2 \\ & \left. + a_{11} + a_{13}X_2^2\Theta_0^2 + a_{13}X_1^2\Theta_0^2\right) d\Omega \end{aligned} \tag{4.29}$$

$$\begin{aligned} E = \int_\Omega & \frac{1}{\left(1 + \Theta_0^2 X_1^2 + \Theta_0^2 X_2^2\right)^2}(-a_{13}X_2^2\Theta_0 - a_{13}X_1^2\Theta_0 + a_{11}X_2^2\Theta_0 + a_{11}X_1^2\Theta_0 \\ & - 2G_{31}X_2^2\Theta_0 - 2G_{31}X_1^2\Theta_0 + 4G_{13}X_1^2 X_2^2\Theta_0^3 - 2a_{33}X_1^2 X_2^2\Theta_0^3 \\ & + 2a_{31}X_1^2 X_2^2\Theta_0^3 - a_{33}X_2^4\Theta_0^3 - a_{33}X_1^4\Theta_0^3 + a_{31}X_2^4\Theta_0^3 + a_{31}X_1^4\Theta_0^3 \\ & \left. + 2G_{13}X_2^4\Theta_0^3 + 2G_{13}X_1^4\Theta_0^3\right) d\Omega \end{aligned} \tag{4.30}$$

$$
\begin{aligned}
F = \int_\Omega \frac{1}{\left(1+\Theta_0^2X_1^2+\Theta_0^2X_2^2\right)^2}(&G_{13}X_1^2X_2^2\Theta_0^3 + G_{31}X_1^2X_2^2\Theta_0^3 + a_{13}X_1^2X_2^2\Theta_0^3 - a_{33}X_1^2X_2^2\Theta_0^3 \\
&- G_{13}\Theta_0X_1^2 + G_{13}\Theta_0^3X_1^4 - G_{31}\Theta_0X_1^2 + G_{31}\Theta_0^3X_1^4 - a_{31}\Theta_0X_1^2 \\
&+ a_{33}X_0^4\Theta_0^3 + a_{11}\Theta_0X_1^2 + a_{13}\Theta_0^3X_1^4)d\Omega
\end{aligned}
\tag{4.31}
$$

$$
\begin{aligned}
G = \int_\Omega \frac{1}{\left(1+\Theta_0^2X_1^2+\Theta_0^2X_2^2\right)^2}(&a_{33}X_2^2\Theta_0^2 + a_{33}X_1^2\Theta_0^2 - a_{21}\Theta_0^2X_2^2 - a_{21}\Theta_0^2X_1^2 \\
&+ 2a_{13}\Theta_0^4X_2^2X_1^2 + a_{23}\Theta_0^2X_2^2 + a_{23}\Theta_0^4X_2^4 + a_{23}\Theta_0^2X_1^2 + a_{23}\Theta_0^4X_1^4 \\
&- 2G_{13}\Theta_0^2X_2^2 - 2G_{13}\Theta_0^2X_1^2 - 2G_{31}\Theta_0^2X_1^2 - 2G_{31}\Theta_0^2X_2^2 + a_{31} + a_{21} \\
&+ 2a_{23}\Theta_0^4X_2^2X_1^2 + a_{11}\Theta_0^2X_2^2 + a_{11}\Theta_0^2X_1^2 + a_{13}\Theta_0^4X_2^4 + a_{13}\Theta_0^4X_1^4)d\Omega.
\end{aligned}
\tag{4.32}
$$

Next, the rod parameters H, A and B can be found from the expression for the internal contact moment. From the strain energy expression, internal contact moment $\mathbf{M}$ is expressed in the following form:

$$
\begin{aligned}
\mathbf{M} &= \frac{\partial\Phi}{\partial\kappa_1}\mathbf{e}_1 + \frac{\partial\Phi}{\partial\kappa_2}\mathbf{e}_2 + \frac{\partial\Phi}{\partial\kappa_3}\mathbf{e}_3 \\
&= (A_1 + F\nu_1)\,\mathbf{e}_1 + (A_2 + F\nu_2)\,\mathbf{e}_2 + \left(E(\nu_3 - 1) + B\kappa_3 + H\left(\frac{a+b}{2} - 1\right)\right)\mathbf{e}_3
\end{aligned}
\tag{4.33}
$$

From the constitutive equations for a hemitropic rod, the internal contact moment can be found as a function of material parameters as:

$$
\mathbf{M} = \mathbf{R}^T \int_\Omega \{X_\alpha \mathbf{RU}\mathbf{e}_\alpha \times (\Sigma_{i3}\mathbf{e}_i)\}\, d\Omega \tag{4.34}
$$

Finally, these rod parameters can be found as:

$$
\begin{aligned}
H = \int_\Omega \frac{1}{\left(1+\Theta_0^2X_1^2+\Theta_0^2X_2^2\right)^2}(&a_{33}X_2^2\Theta_0 + a_{33}X_1^2\Theta_0 - a_{31}X_2^2\Theta_0 - a_{31}X_1^2\Theta_0 \\
&+ a_{23}X_2^2\Theta_0 + a_{23}X_1^2\Theta_0 - a_{21}X_2^2\Theta_0 - a_{21}X_1^2\Theta_0 + a_{23}X_2^4\Theta_0^3 + a_{23}X_1^4\Theta_0^3 \\
&- a_{21}X_2^4\Theta_0^3 - a_{21}X_1^4\Theta_0^3 + a_{13}X_2^4\Theta_0^3 + a_{13}X_1^4\Theta_0^3 - a_{11}X_2^4\Theta_0^3 - a_{11}X_2^4\Theta_0^3 \\
&- 2G_{31}X_2^2\Theta_0 + 2a_{23}X_2^2X_1^2\Theta_0^3 - 2a_{21}X_2^2X_1^2\Theta_0^3 + 2a_{13}X_2^2X_1^2\Theta_0^3 - 2a_{11}X_2^2X_1^2\Theta_0^3 \\
&- 2G_{31}X_1^2\Theta_0 + 2G_{13}X_2^4\Theta_0^3 + 2G_{13}X_1^4\Theta_0^3 + -4G_{13}X_1^2X_2^2\Theta_0^3)d\Omega
\end{aligned}
\tag{4.35}
$$

$$
\begin{aligned}
A = \int_\Omega \frac{1}{\left(1+\Theta_0^2X_1^2+\Theta_0^2X_2^2\right)^2}(&a_{31}X_2^4\Theta_0^2 + a_{33}X_2^6\Theta_0^4 + 2G_{13}X_2^4\Theta_0^2 \\
&+ 2G_{31}X_2^4\Theta_0^2 + a_{13}X_2^4\Theta_0^2 + a_{11}X_2^2 + 2G_{13}X_1^2X_2^2\Theta_0^2 + G_{31}X_1^2X_2^2\Theta_0^2 \\
&+ a_{31}X_1^2X_2^2\Theta_0^2 + 2a_{33}X_1^2X_2^4\Theta_0^4 + a_{33}X_1^4X_2^2\Theta_0^4 + a_{13}X_1^2X_2^2\Theta_0^2)d\Omega
\end{aligned}
\tag{4.36}
$$

$$
\begin{aligned}
B = \int_\Omega \frac{1}{\left(1+\Theta_0^2X_1^2+\Theta_0^2X_2^2\right)^2}(&-G_{13}X_1^4\Theta_0^2 - G_{31}X_1^4\Theta_0^2 - G_{13}X_2^4\Theta_0^2 - G_{31}X_2^4\Theta_0^2 \\
&- a_{13}X_1^4\Theta_0^2 - a_{13}X_2^4\Theta_0^2 + a_{11}X_1^4\Theta_0^2 + a_{11}X_2^4\Theta_0^2 + a_{33}X_2^4\Theta_0^2 \\
&+ a_{33}X_1^4\Theta_0^2 - a_{31}X_2^4\Theta_0^2 - a_{31}X_1^4\Theta_0^2 + 2a_{33}X_1^2X_2^2\Theta_0^2 \\
&- 2a_{31}X_1^2X_2^2\Theta_0^2 - 2a_{13}X_1^2X_2^2\Theta_0^2 + 2a_{11}X_1^2X_2^2\Theta_0^2 - 2G_{31}X_1^2X_2^2\Theta_0^2 \\
&- 2G_{13}X_1^2X_2^2\Theta_0^2 + 3G_{13}X_1^2X_2^4\Theta_0^4 + 3G_{13}X_1^4X_2^2\Theta_0^4 \\
&+ G_{31}X_2^2 + G_{31}X_1^2 + G_{13}X_2^6\Theta_0^4 + G_{13}X_1^6\Theta_0^4)d\Omega
\end{aligned}
\tag{4.37}
$$

I and J can be found from internal conjugate force q_1. From strain energy expression, q_1 can be expressed as

$$
q_1 = \frac{\partial\Phi}{\partial a} = \frac{J}{2}(b-1) + \frac{I}{4}(a-1) + \frac{I}{4}(b-1) + \frac{G+H}{2}(\nu_3 - 1). \tag{4.38}
$$

From internal conjugate force expression, q_1 can also be expressed as

$$
q_1 = -\mathbf{e}_1 \cdot \left\{\kappa \times \int_\Omega X_1\Sigma_{i3}\mathbf{e}_i d\Omega\right\} + \int_\Omega \mathbf{e}_1 \cdot \Sigma_{i1}\mathbf{e}_i d\Omega. \tag{4.39}
$$

Then, rod parameters I and J can be expressed as follows:

$$
\begin{aligned}
I = \int_{\Omega} & \frac{4}{\left(X_1^2 + X_2^2\right)^2 \left(1 + \Theta_0^2 X_1^2 + \Theta_0^2 X_2^2\right)^2} (a_{21} X_1^4 X_2^2 \Theta_0^2 + a_{23} X_1^2 X_2^4 \Theta_0^2 \\
& + a_{21} X_1^6 X_2^2 \Theta_0^4 + 2a_{21} X_1^4 X_2^4 \Theta_0^4 + 2a_{22} X_1^6 \Theta_0^2 + a_{22} X_1^8 \Theta_0^2 4G_{12} X_1^4 X_2^4 \Theta_0^4 + 2G_{21} X_1^4 X_2^2 \Theta_0^2 \\
& + 2G_{21} X_1^2 X_2^4 \Theta_0^2 + 2G_{23} X_2^4 X_1^2 \Theta_0^2 + 2G_{21} X_1^2 X_2^6 \Theta_0^4 + 2G_{32} X_1^2 X_2^2 + a_{32} X_1^2 X_2^4 \Theta_0^2 \\
& + a_{32} X_1^4 X_2^2 \Theta_0^2 + a_{31} X_1^2 X_2^4 \Theta_0^2 + a_{32} X_1^2 X_2^2 + a_{23} X_1^2 X_2^2 + 2G_{12} X_1^2 X_2^6 \Theta_0^4 + a_{12} X_1^2 X_2^6 \Theta_0^4 \\
& + 2a_{12} X_1^4 X_2^4 \Theta_0^4 + a_{12} X_1^4 X_2^2 \Theta_0^2 + a_{12} X_1^6 X_2^2 \Theta_0^4 + a_{12} X_2^4 X_1^2 \Theta_0^2 + 2a_{11} X_1^2 X_2^6 \Theta_0^4 + a_{11} X_1^4 X_2^4 \Theta_0^4 \\
& + a_{13} X_1^2 X_2^4 \Theta_0^2 + a_{31} X_2^6 \Theta_0^2 + 2G_{12} X_1^2 X_2^4 \Theta_0^2 + 2G_{21} X_1^6 X_2^2 \Theta_0^4 + 2G_{12} X_1^4 X_2^2 \Theta_0^2 \\
& + 4G_{21} X_1^4 X_2^4 \Theta_0^4 + 2G_{31} X_1^2 X_2^4 \Theta_0^2 + 2G_{32} X_1^4 X_2^2 \Theta_0^2 + 2G_{32} X_1^2 X_2^4 \Theta_0^2 + a_{33} X_2^4 \\
& + a_{22} X_1^4 X_2^4 \Theta_0^4 + 2G_{12} X_1^6 X_2^2 \Theta_0^4 + 2G_{23} X_1^4 X_2^2 \Theta_0^2 + a_{21} X_1^2 X_2^4 \Theta_0^2 + a_{21} X_1^2 X_2^6 \Theta_0^4 \\
& + 2a_{22} X_1^4 X_2^2 \Theta_0^2 + a_{23} X_1^4 X_2^2 \Theta_0^2 + a_{11} X_2^8 \Theta_0^4 + a_{13} X_2^6 \Theta_0^2 + a_{22} X_1^4 \\
& + 2G_{13} X_1^2 X_2^4 \Theta_0^2 + 2a_{22} X_1^6 X_2^2 \Theta_0^4 + 2G_{31} X_2^6 \Theta_0^2 + 2G_{23} X_1^2 X_2^2 + 2G_{13} X_2^6 \Theta_0^2) d\Omega,
\end{aligned}
\tag{4.40}
$$

$$
\begin{aligned}
J = \int_{\Omega} & \frac{-2}{\left(X_1^2 + X_2^2\right)^2 \left(1 + \Theta_0^2 X_1^2 + \Theta_0^2 X_2^2\right)^2} (a_{21} X_1^4 X_2^2 \Theta_0^2 + a_{21} X_1^6 X_2^2 \Theta_0^4 + a_{21} X_1^4 X_2^4 \Theta_0^4 \\
& - a_{21} X_2^6 \Theta_0^2 - a_{21} X_2^8 \Theta_0^4 + 2a_{22} X_1^6 \Theta_0^2 + a_{22} X_1^8 \Theta_0^4 - a_{23} X_2^6 \Theta_0^2 + 8G_{12} X_1^4 X_2^4 \Theta_0^4 \\
& + 4G_{21} X_1^4 X_2^2 \Theta_0^2 + 4G_{21} X_1^2 X_2^4 \Theta_0^2 + 4G_{23} X_2^4 X_1^2 \Theta_0^2 + 4G_{21} X_1^2 X_2^6 \Theta_0^4 + 2G_{32} X_1^2 X_2^2 \\
& + a_{32} X_1^2 X_2^4 \Theta_0^2 + a_{32} X_1^4 X_2^2 \Theta_0^2 + a_{31} X_1^2 X_2^4 \Theta_0^2 + a_{32} X_1^2 X_2^2 + a_{23} X_1^2 X_2^2 + 4G_{12} X_1^2 X_2^6 \Theta_0^4 \\
& - a_{13} X_1^4 X_2^2 \Theta_0^2 - a_{22} X_1^2 X_2^2 + a_{12} X_1^2 X_2^6 \Theta_0^4 + a_{12} X_1^4 X_2^4 \Theta_0^4 - a_{11} X_1^6 X_2^2 \Theta_0^4 - a_{12} X_1^6 X_2^2 \Theta_0^4 \\
& + a_{12} X_1^2 X_2^4 \Theta_0^2 + a_{11} X_1^2 X_2^6 \Theta_0^4 - a_{11} X_1^4 X_2^4 \Theta_0^4 - a_{32} X_1^6 \Theta_0^2 + a_{31} X_2^6 \Theta_0^2 + 4G_{12} X_1^2 X_2^4 \Theta_0^2 \\
& + 4G_{21} X_1^6 X_2^2 \Theta_0^4 + 4G_{12} X_1^4 X_2^2 \Theta_0^2 + 8G_{21} X_1^4 X_2^4 \Theta_0^4 + 4G_{32} X_1^4 X_2^2 \Theta_0^2 + 4G_{32} X_1^2 X_2^4 \Theta_0^2 + a_{33} X_1^4 \\
& - a_{32} X_1^4 - a_{22} X_1^4 X_2^4 \Theta_0^4 - a_{22} X_1^2 X_2^6 \Theta_0^4 + 4G_{12} X_1^6 X_2^2 \Theta_0^4 + 4G_{23} X_1^4 X_2^2 \Theta_0^2 - a_{21} X_1^2 X_2^6 \Theta_0^4 \\
& - 2G_{13} X_1^4 X_2^2 \Theta_0^2 + a_{23} X_1^4 X_2^2 \Theta_0^2 + a_{11} X_2^8 \Theta_0^4 - a_{12} X_1^6 \Theta_0^2 - a_{12} X_1^8 \Theta_0^4 + a_{13} X_2^6 \Theta_0^2 \\
& + a_{22} X_1^4 - a_{23} X_2^4 - 2G_{31} X_1^4 X_2^2 \Theta_0^2 - 2a_{22} X_1^2 X_2^4 \Theta_0^2 + a_{22} X_1^6 X_2^2 \Theta_0^4 + 2G_{31} X_2^6 \Theta_0^2 \\
& + 4G_{23} X_1^2 X_2^2 + 2G_{13} X_2^6 \Theta_0^2) d\Omega.
\end{aligned}
\tag{4.41}
$$

Rod parameters K and L could be found from interal conjugate force expression Q_1. From the strain energy expression, Q_1 has the following form:

$$
Q_1 = \frac{\partial \Phi}{\partial a'} = \frac{k}{2}(a' + b') + \frac{L}{2} b'. \tag{4.42}
$$

Q_1 as an internal force conjugated to a' can also be expressed as

$$
Q_1 = \int_{\Omega} (X_1 \mathbf{e}_1 \cdot \Sigma_{i3} \mathbf{e}_i) d\Omega. \tag{4.43}
$$

Finally, the expressions of K and L are:

$$K = \int_{\Omega} \frac{4}{\left(X_1^2 + X_2^2\right)^2 \left(1 + \Theta_0^2 X_1^2 + \Theta_0^2 X_2^2\right)^2} (-G_{31} X_1^4 X_2^2 \Theta_0^2 - a_{31} X_1^4 X_2^2 \Theta_0^2 + a_{33} X_1^4 X_2^2 \Theta_0^2$$
$$- G_{13} X_2^4 X_1^2 \Theta_0^2 + G_{13} X_2^6 X_1^2 \Theta_0^4 + a_{11} X_2^2 X_1^4 \Theta_0^2 + G_{21} X_1^6 \Theta_0^2 + G_{23} X_1^6 \Theta_0^2$$
$$+ G_{23} X_1^8 \Theta_0^4 - G_{31} X_1^2 X_2^4 \Theta_0^2 + 2G_{13} X_1^4 X_2^4 \Theta_0^4 + G_{13} X_1^6 X_2^2 \Theta_0^4 - G_{13} X_1^4 X_2^2 \Theta_0^2$$
$$+ G_{21} X_1^4 X_2^2 \Theta_0^2 + G_{23} X_1^4 X_2^2 \Theta_0^2 + 2G_{23} X_1^6 X_2^2 \Theta_0^4 + G_{23} X_1^4 X_2^4 \Theta_0^4 + a_{11} X_1^2 X_2^4 \Theta_0^2$$
$$- a_{13} X_1^2 X_2^4 \Theta_0^2 - a_{31} X_1^2 X_2^4 \Theta_0^2 + a_{33} X_1^2 X_2^4 \Theta_0^2 + G_{21} X_1^4 + G_{31} X_1^2 X_2^2 - a_{13} X_1^4 X_2^2 \Theta_0^2) d\Omega, \tag{4.44}$$

$$L = \int_{\Omega} \frac{-2}{\left(X_1^2 + X_2^2\right)^2 \left(1 + \Theta_0^2 X_1^2 + \Theta_0^2 X_2^2\right)^2} (2G_{31} X_1^2 X_2^2 + G_{21} X_1^4 - 2G_{31} X_1^4 X_2^2 \Theta_0^2 - 2G_{13} X_1^4 X_2^2 \Theta_0^2$$
$$+ 4G_{13} X_1^4 X_2^4 \Theta_0^4 + 2G_{13} X_1^6 X_2^2 \Theta_0^4 + G_{23} X_1^6 X_2^2 \Theta_0^4 - G_{23} X_1^4 X_2^4 \Theta_0^4 - G_{21} X_1^2 X_2^2 - G_{21} X_1^2 X_2^4 \Theta_0^2$$
$$- G_{23} X_1^2 X_2^4 \Theta_0^2 + 2a_{11} X_1^4 X_2^2 \Theta_0^2 - 2a_{13} X_1^4 X_2^2 \Theta_0^2 - 2a_{31} X_1^4 X_2^2 \Theta_0^2 + 2a_{33} X_1^4 X_2^2 \Theta_0^2 + 2a_{11} X_1^2 X_2^4 \Theta_0^2$$
$$- 2a_{13} X_1^2 X_2^4 \Theta_0^2 - 2a_{31} X_1^2 X_2^4 \Theta_0^2 + 2a_{33} X_1^2 X_2^4 \Theta_0^2 - 2G_{13} X_1^2 X_2^4 \Theta_0^2 - 2G_{31} X_1^2 X_2^4 \Theta_0^2$$
$$- G_{23} X_1^2 X_2^6 \Theta_0^4 + G_{21} X_1^6 \Theta_0^2 + G_{23} X_1^6 \Theta_0^2 + G_{23} X_1^8 \Theta_0^4 + 2G_{13} X_1^2 X_2^6 \Theta_0^4) d\Omega. \tag{4.45}$$

Now, we derived all twelve rod parameters in term of five material parameters and Chirality angle. The five material parameters could be estimated from an inverse approach give the twelve rod parameters.

4.3.3 Special Case of Armchair SWNT

In the previous section, twelve rod parameters are derived for Chiral SWNT. As for Armchair SWNT, it could be treat as a special case of Chiral SWNT with primary material direction parallel to the axis of SWNT. This is equivalent to set

$\Theta_0 = 0$. Then the following rod parameters for Armchair SWNT could be found as

$$A = a_{11}\bar{I}$$

$$B = \bar{G}\bar{J}$$

$$C = \bar{G}\bar{A}$$

$$D = a_{11}\bar{A}$$

$$E = 0$$

$$F = 0$$

$$G = (a_{21} + a_{31})\bar{A}$$

$$H = 0$$

$$I = 6\pi a_{22}t + 4\pi Gt + 2\pi a_{32}t$$

$$J = -4\pi Gt + 2\pi a_{22}t - 2\pi a_{32}t$$

$$K = 4\bar{G}\bar{I}$$

$$L = -2\bar{G}\bar{I}$$

Here, t denotes the wall thickness of a SWNT. The radial modulus is $I+J = 4a_{22}\bar{A}$. Three coupling moduli E, F and H vanish here. E is the coupling coefficient between extension and twist. F is the coupling coefficient between shear and bending. H is the coupling coefficient between twist and Poission effect. This is in agreement with numerial and experimental results that armchair SWNT does not show coupling between these deformation modes.

4.4 Conclusions

A mathematically consistent extension to the aformensioned rod theory is developed that connect an isotropic and a hemitropic rod by exploring material symmetry. This proposed approach is applied to model SWNTs with different chirality. It effectively connects the modeling of different types of SWNT using five material parameters. The connection between different types of SWNT is controled by the chirality angle in the previous derivation. Future effort could involve solving the inverse problem to find these material parameters.

CHAPTER 5

CONCLUSIONS AND FUTURE WORK

This dissertation is primarily motivated by both theoretical and computational challenges associated with the Cosserat rod model. The finite element approach is developed for standard and revised Cosserat rod models with several numerical examples to study the behavior of SWNT deformation such as buckling of SWNT and coupling behavior of deformations modes. Futhermore, an analytical study is performed to address a major disadvantage of the rod model. A unified form for all types of SWNT is proposed in this work.

In Chapter 2, a FEM model for deformation of SWNTs, subjected to axial and transverse forces, bending moments and torques, is presented in this work. This analysis is based on a quadratic expression (2.18) for strain energy per unit undeformed length of a rod. The resulting constitutive model for the SWNT is anisotropic. Geometric and material nonlinearities are included in this model. Finally, a recent experimental paper is revisted using the solver developed.

In Chapter 3, a FEM implementation of an atomistic continuum model, based on an extended Cosserat rod theory, for mechanical deformation of a SWNT, is proposed. Geometric nonlinearity is included in the FEM implementation. Two kinds of problems are considered in the numerical examples - coupling of extension, twist and cross-sectional deformation of a (9,6) chiral SWNT and Euler buckling of a (10,10) armchair SWNT. This numerical implimentation provides a strong and complete tool set to study the deformation of SWNTs.

In the next Chapter, an analytical study is performed to connect modeling of

SWNTs with different chiralities. An unified expression of a rod model for all types of SWNTs is proposed by exploring material symmetry of SWNTs. This approach addresses a major disadvantage of the Cosserat rod model when modeling SWNTs.

Future work will be needed to solve an inverse problem and find the new material parameters. More fundamental studies of Cosserat rod model is be needed as well. For example, a quadratic energy form is adopted for the Cosserat rod model in this thesis and higher order energy terms are dropped. These higher order of energy terms are useful for modeling some local behavior of SWNTs such as local surface buckling. It would be useful to incorporate these higher order terms in future work. The model in this thesis can be applied to other applications of rod models e.g., DNA, fiber reinforced composite rods, etc.

BIBLIOGRAPHY

[1] Antman, S.S., 1995. Nonlinear problems of elasticity. Springer-Verlag, New York.

[2] Arroyo, M., Belytschko, T., 2004. Finite crystal elasticity of carbon nanotubes based on the exponential Cauchy-Born rule. Phys. Rev. B 69, 115415.

[3] Belytschko, T., Xiao, S.P., Schatz, G.C., Ruoff, R.S., 2002, "Atomistic Simulations of Nanotube Fracture", Phys, Rev, B 65, 235430(1-8)

[4] Brenner, D.W., Shenderova, O.A., Harrison, J.A., Stuart, S.J., Ni, B., Sinnott, S.B., 2002. A second-generation reactive empirical bond order (REBO) potential energy expression for hydrocarbons. J. Phys.: Condens. Matter 14, 783-802.

[5] Buehler, M., Kong, Y., Gao, H., 2004. Deformation mechanisms of very long single-wall carbon nanotubes subject to compressive loading. J. Eng. Mater. Technol., 126, 245-249.

[6] Buehler, M., 2006. Mesoscale modeling of mechanics of carbon nanotubes: Self Assembly, self-folding, and fracture. J. Mater. Res., 21, 2855-2869.

[7] Chandraseker, K., Mukherjee, S., Mukherjee, Y.X., 2006. Modifications to the Cauchy-Born rule: Applications in the deformation of single-walled carbon nanotubes. Int. J. Solids. Struct. 43, 7128-7144.

[8] Chandraseker, K., Mukherjee, S., 2006. Coupling of extension and twist in single-walled carbon nanotubes.J. App Mech. 73 (2), 315-326.

[9] Chandraseker, K., Mukherjee, S., 2007. Atomistic-continuum and ab initio estimation of the elastic moduli of single-walled carbon nanotubes. Comput. Mater. Sci. 40, 147-158.

[10] Chandraseker, K., and Mukherjee, S., Paci, J. T., Schatz, G. C., 2009. An atomistic-continuum Cosserat rod model of carbon nanotubes, J. Mech. Phys. Solids, 57, pp. 932-958.

[11] Chang, T. 2010. A molecular based anisotropic shell model for single-walled carbon nanotubes. J. Mech. Phys. Solids 58, pp. 1422-1433.

[12] Cramer, C.J., 2004. Essentials of Computational Chemistry: Theories and Models. Wiley, Ed. 2.

[13] Dayal K., James, R.D., 2010. Nonequilibrium molecular dynamics for bulk materials and nanostructures, J. Mech. Phys. Solids, 58, 145-163.

[14] Dresselhaus, M.S., Dresselhaus, G., Jorio, A., 2004. Unusual properties and structure of carbon nanotubes. Annu. Rev. Mater. Res. 34, 247-278.

[15] Elstner, M., Porezag, D., Jungnickel, G., Elsner, J., Haugk, M., Frauenheim, Th., 1998. Self-consistent-charge density-functional tight-binding method for simulations of complex materials properties. Phys. Rev. B 58(11), 7260-7268.

[16] Fang, C., Kumar, A., Mukherjee, S., 2011. A finite element analysis of single-walled carbon nanotube deformation. J. App Mech. 78, 034502.

[17] Frauenheim, Th., Seifert, G., Elstner, M., Niehaus, T., Köhler, C., Amkreutz, M., Sternberg, M.,Hajnal, Z., Di Carlo, A., Suhai, S., 2002. Atomistic simulations of complex materials: ground-state and excited-state properties. Journal of Physics: Condensed Matter 14, 3015-3047.

[18] Gartstein, Yu.N., Zakhidov, A.A., Baughman, R.H., 2003. Mechanical and electromechanical coupling in carbon nanotube distortions. Phys. Rev. B 68, 115415.

[19] Gautieri, A., Buehler, M.J., Redaelli, A., 2009. Deformation rate controls elasticity and unfolding pathway of single tropocollagen molecules. Journal of the Mechanical Behavior of Biomedical Materials 2, 130-137.

[20] Gould, T., Burton, D.A., 2006. A Cosserat rod model with microstructure. New J. Phys. 8, 137(1-17).

[21] Govindjee, S., Sackman, J.L., 1999. On the use of continuum mechanics to estimate the properties of nanotubes. Solid State Comm. 110, 227-230.

[22] Healey, T.J., 2002. Material symmetry and chirality in nonlinearly elastic rods. Mathematics and Mechanics of Solids 7, 405-420.

[23] Hohenberg, P., Kohn, W., 1964. Inhomogeneous electron gas. Phys. Rev. 136, B864.

[24] Iijima, S., Brabec, C., Maiti, A., Bernholc, J., 1996. Structural flexibility of carbon nanotubes. J. Chem. Phys. 104, 2089-2092.

[25] James, R. D., 2006. Objective Structures. J. Mech. Phys. Solids, 54, pp. 2354-2390.

[26] Jiang, H., Zhang, P., Liu, B., Huang, Y., Geubelle, P.H., Gao, H., Hwang, K.C.,2003. The effect of nanotube radius on the constitutive model for carbon nanotubes.J. Comput. Master. Sci. 28, 429-442.

[27] Jiang, H., Feng, X.-Q., Huang, Y., Hwang, K.C., Wu, P.D., 2004. Defect nucleation in carbon nanotubes under tension and torsion: Stone-wales transformation. Comput. Methods Appl. Mech. Engrg. 193, 3419-3429.

[28] Kohn, W., Sham, L.J., 1965. Self-consistent equations including exchange and correlation effects. Phys. Rev. 140, A1133.

[29] Kong, J., Franklin, N. R., Zhou, C., Chapline, M. G., Peng, S., Cho, K., Dai, H.,2000. Nanotube molecular wires as chemical sensors. Science 287, 622-625.

[30] Kumar, A., Healey, T.J., 2010. A generalized computational approach to stability of static equilibria of nonlinearly elastic rods in the presence of constraints. Comp. Methods App. Mech. Engrg 199, 1805-1815.

[31] Kumar, A., Mukherjee, S., 2011. A Geometrically Exact Rod Model including in-plane cross-sectional deformation. J. App Mech. 78, 011010.

[32] Kumar, A., Mukherjee, S., Paci, T.J., Chandraseker, K., Schatz, C.G., 2011. A rod model for three dimensional deformations of Single-walled carbon nanotubes. Int. J. Solids Struct., 48, 2849-2858.

[33] Kumar, A., 2012, An atomistic based finite deformation rod model for single-walled carbon nanotube. (submitted for publication)

[34] Lennard-Jones, J.E., 1931. Cohesion. Proceedings of the Physical Society 43, 461-482.

[35] Li, C., Chou, T.-W., 2004. Vibrational behaviors of multiwalled-carbon-nanotube-based nanomechanical resonators. App. Phys. Lett. 84, 121-123.

[36] Liang, H., Upmanyu, M., 2006. Axial-strain-induced torsion in single-walled carbon nanotubes. Phys. Rev. Lett. 96, 165501(1-4).

[37] Liew, K. M., Wong, C. H., Tan, M., J., 2006. Twisting effects of carbon nanotube bundles subjected to axial compression and tension. J. App. Phys, 99, 114312.

[38] Liu, B., Jiang, H., Johnson, H.T., Huang, Y., 2004. The influence of mechanical deformation on the electrical properties of single wall carbon nanotubes. J. Mech. Phys. Solids 52, 1-26.

[39] Lourie, O., Cox, D. M., and Wagner, H. D., 1998, "Buckling and Collapse of Embedded Carbon Nanotubes", Phys. Rev. Lett. 81, 1638-1641

[40] Lu, J.P., 1997. Elastic properties of carbon nanotubes and nanoropes. Phys. Rev. Lett. 79, 1297-1300.

[41] Ya-Qiong X., Arthur B., and McEuen P., 2009 "Bending and Twisting of Suspended Single-Walled Carbon Nanotubes in Solution", ASAP Nano Lett., 9 pp 1609-1614

[42] Pantano, A., Boyce, M. C., Parks, D. M., 2004, "Mechanics of Axial Compression of Single and Multi-walled Carbon Nanotubes", J. Eng. Mater. Technol., 126, pp. 279-289.

[43] Qian, D., Dickey, E. C., Andrews, R., Rantell, T., 2000. Load transfer and deformation mechanisms in carbon nanotube-polysterene composites. Appl. Phys. Lett. 76, 2868.

[44] Ru, C.Q., 2000. Effective bending stiffness of carbon nanotubes. Phys. Rev. B 62, 9973-9976.

[45] Sáncez-Portal, D., Artacho, E., Soler, J.M., Rubio, A., Ordejón, P., 1999. *Ab initio* structural, elastic, and vibrational properties of carbon nanotubes. Phys. Rev. B 59, 12678.

[46] Sazonova, V., Yaish, Y., Üstünel, H., Roundy, D., Arias, T.A., McEuen, P.L., 2004. A tunable carbon nanotube electromechanical oscillator. Nature 431, 284-287.

[47] Shenoy, V., Miller, R., Tadmor, E., Rodney, D., Phillips, R., Ortiz, M., 1999. An adaptive finite element approach to atomic-scale mechanics – the quasicontinuum method. J. Mech. Phys. Solids 47, 611-642.

[48] Simo, J. C., and Vu-Quoc, L., 1986, A three-dimensional finite-strain rod model. Part2: computational aspects, Comput. Methods Appl. Mech. Eng., 58,pp. 79-116.

[49] Simo, J. C., and Vu-Quoc, L., 1991, A Geometrically-Exact Rod Model Incorporating Shear and Torsion-Warping Deformation, Int. J. Solids Struct., 27, 371-393.

[50] Stuart, S.J., Tutein, A.,B., Harrison, J.,A., 2000. A reactive potential for hydrocarbons with intermolecular interactions, J. Chem. Phys., 112, 6472.

[51] Tadmor, E.B., Smith, G.S., Bernstein, N., Kaxiras, E., 1999. Mixed finite element and atomistic formulation for complex crystals. Phys. Rev. B 59, 235-245.

[52] Tersoff, J., 1988. New empirical approach for the structure and energy of covalent systems. Phys. Rev. B 37, 6991-7000.

[53] van Duin, C., T., Dasgupta, S., Lorant, F., Goddard, W., A., 2001. ReaxFF:A Reactive Force Field for Hydrocarbons. J. Phys. Chem. A, 105, 9396-9409.

[54] Wang, L., Ni, Q., Li, M., Qian, Q., 2008. The thermal effect on vibration and instability of carbon nanotubes conveying fluid. Physica E. 40, 3179-3182.

[55] Wu, J., Hwang, K. C., Huang, Y., 2008. An Atomistic-based finite deformation shell theory for single-wall carbon nanotubes. J. Mech. Phys. Solids 56, 279-292.

[56] Xiao, T., Xu, X., Liao, K., 2004, "Characterization of Nonlinear Elasticity and Elastic Instability in Single-walled Carbon Nanotubes", J. Appl. Phys. 95, 8145-8148

[57] Yakobson, B.I., Brabec, C.J., Bernholc, J., 1996. Nanomechanics of carbon tubes: Instabilities beyond linear response. Phys. Rev. Lett. 76, 2511-2514.

[58] Yu, M., Louire, O., Dyer, M. J., Moloni, K., Kelly, T. F., Ruoff, R. S., 2000. Strength and Breaking Mechanism of Multiwalled Carbon Nanotubes under tensile load. Science 287, 637-640.

[59] Yu, M.-F., 2004. Fundamental mechanical properties of carbon nanotubes: Current understanding and the related experimental studies. J. Engg. Mat. Technol. 126, 271-278.

[60] Yurdumakan, B., Raravikar, N., R., Pulickel, M., A., Dhinojwala, A., 2005. Synthetic gecko-foot hairs from multiwalled carbon nanotubes. Chem. Commun. 30, 3799-3801.

[61] Zhang, P., Huang, Y., Geubelle, P.H., Klein, P.A., Hwang, K.C., 2002. The elastic modulus of single-wall carbon nanotubes: A continuum analysis incorporating interatomic potentials. Int. J. Solids Struct. 39, 3893-3906.

[62] Zhang, Y., Liu, G., Han, X., 2005. Transverse vibrations of double-walled carbon nanotubes under compressive axial load. Phys. Lett. A 340, 258-266.

[63] Zhao, H., Min, K., Aluru, N.R., 2009. Size and Chirality Dependent Elastic Properties of Graphene Nanoribbons under Uniaxial Tension. Nano Lett. 9, 3012-3015.

[64] Zhou, W., Huang, Y., Liu, B., Hwang, K.C., Zuo, J.M., Buehler, M.J., Gao,

H., 2007. Self-folding of single and multiwall carbon nanotubes. Appl. Phys. Lett. 90, 073107.

[65] Zou, J., Huang, X., Arroyo, M., Zhang, S., 2009. Effective coarse-grained simulations of super-thick multi-walled carbon nanotubes under torsion. J. App. Phy, 105, 033516.